Noelia Hurtado López-Plaza

Modelling of a vector-controlled bearingless synchronous reluctance motor drive

School of Electrical Engineering

Espoo September 10, 2014

Project supervisor:

Prof. Marko Hinkkanen

Aalto University
School of Electrical
Engineering

AALTO UNIVERSITY
SCHOOL OF ELECTRICAL ENGINEERING

ABSTRACT OF
THE FINAL
PROJECT

Author: Noelia Hurtado López-Plaza

Title: Modelling of a vector-controlled bearingless synchronous reluctance motor drive

Date: September 10, 2014 Language: English Number of pages:9+47

Department of Electrical Engineering and Automation

Professorship: Electric Drives Code: S-81

Supervisor and instructor: Prof. Marko Hinkkanen

This final project deals with the modelling of a vector-controlled bearingless synchronous reluctance motor (BSyRM) drive. The goal of this project is to develop the dynamic model of a BSyRM. A brief introduction going through the advantages and disadvantages of conventional machines shows the importance of BSyRMs development. An explanation about the general aspects and operating principles of BSyRMs is presented together with the general dynamic model equations of the permanent-magnets synchronous machine. Several assumptions are considered to adapt the permanent-magnets machine model to the BSyRM model desired. The description of the controllers employed in the vector control implementation is also included. The study is made through a literature review and by simulation using the Matlab/Simulink software. The implementation of the BSyRM dynamic model and vector control and the simulation results are presented. Simulations show that the model developed is well suited for the BSyRM.

Keywords: Bearingless synchronous reluctance motor, motor windings, suspension windings, radial force, vector control

AALTO UNIVERSITY
SCHOOL OF ELECTRICAL ENGINEERING

ABSTRACT DEL PROYECTO FIN DE CARRERA

Autor: Noelia Hurtado López-Plaza

Título: Modelado de un motor síncrono de reluctancia sin rodamientos controlado vectorialmente

Fecha: September 10, 2014 Idioma: Inglés Número de páginas:9+47

Departamento de Ingeniería Eléctrica y Automática

Cátedra: Vehículos Eléctricos Código: S-81

Tutor: Prof. Marko Hinkkanen

Este proyecto final de carrera aborda el modelado de un motor síncrono de reluctancia sin rodamientos controlado vectorialmente. El objetivo del proyecto es el desarrollo del modelo dinámico del motor síncrono de reluctancia sin rodamientos. Una breve introducción repasando las ventajas e inconvenientes de los motores convencionales, nos muestra la importancia del desarrollo de motores sin rodamientos. El proyecto incluye la definición de los aspectos más generales y principios de funcionamiento de este tipo de motores, junto con las ecuaciones generales del modelo dinámico del motor síncrono de imanes permanentes. Distintas suposiciones son llevadas a cabo para adaptar las ecuaciones del modelo de imanes permanentes al modelo síncrono de reluctancia sin rodamientos deseado. La descripción detallada del control vectorial empleado en la realización del proyecto también se incluye. El estudio se ha llevado a cabo mediante la revisión de la literatura previa referente al tema y de varias simulaciones en el entorno Matlab/Simulink. La construcción del modelo dinámico y del control vectorial del motor junto con los resultados de las simulaciones, son incluidos en el proyecto. Los resultados que se presentan muestran como el modelo desarrolado es adecuado para los motores síncronos de reluctancia sin rodamientos.

Palabras clave: Motor síncrono de reluctancia sin rodamientos, bobinados del motor, bobinados de la suspensión, fuerza radial, control vectorial

Preface

The work of this Final Project was done in the Electric Drives group, on the Department of Electrical Engineering and Automation at the School of Electrical Engineering of the Aalto University, in Helsinki, Finland. The group is led by Professor Marko Hinkkanen.

I am very grateful to my supervisor Prof. Marko Hinkkanen, for giving me the opportunity of joining this project and trust me. His support and advices in our long meetings have been very important to keep on working every day with illusion.

I would also like to express my gratitude to my office mates, specially Jarno, Jussi and Elahe. You were always willing to help me with any problem I had.

A special mention to my Erasmus family, thank you for all the moments we have lived together, without all of you this experience would have never been the same. A very special mention to my "Gorditos", Nicola and Alberto, thank you for being as you are and for all the funny/crazy moments full of laughter and for others full of tears, you know this is just the beginning of our adventure.

Alicia and Coco, my dear flatmates, with whom I have been living almost one year, I could not have been luckier, you are the best company anybody can have. Thank you cutie for taking care of me and being my confident, for all the moments we shared, our travels, parties and deep conversations in the early morning.

Bea, with whom I spent the best and worse moments of the degree at ETSIIM. After too many hours studying at university, now we can say we have achieved it, we are engineers!. I am also very grateful to the UPM for giving me the chance to come to Finland and improve as person and as engineer.

Finally, my deepest appreciation goes to my family, for their endless support during all these years and for every time we share. To my mum, Mª José, and to my dad, Manuel, for being there for me in good and bad times always with wise words, and to my brother, Jorge, that I am sure will become an important physicist. To Pirata for the happy moments he gave us and to Cala for making us smile again. To my grandparents, Adela and Cipriano, for teaching me that there are still good persons in the world. And my last words to Gabri, for giving me these wonderful months and support me every day with a smile on his face, thank you "campeón".

"Do not be sad because it is over, be happy because it happened"

Otaniemi, September 9, 2014.

Noelia Hurtado López-Plaza

Contents

Symbols and abbreviations

Symbols

$\boldsymbol{e}_m$	Back-EMF
$\boldsymbol{F}_{ij}$	Radial force vector in rotating coordinates
F_i	Radial force i-axis
F_j	Radial force j-axis
$\boldsymbol{F}_{xy}$	Radial force vector in stationary coordinates
F_x	Radial force x-axis
F_y	Radial force y-axis
F_c	Transfer function PI-controller
$\boldsymbol{F}_{c,m}$	PI-type motor current controller
$\boldsymbol{F}_{c,s}$	PI-type suspension current controller
G_{cc}	General closed-loop transfer function
G_e	General transfer function
$\boldsymbol{G}_{e,m}$	Motor transfer function matrix
$\boldsymbol{G}_{e,s}$	Suspension transfer function matrix
i	Rotating reference i-axis
$\boldsymbol{i}$	General current space vector
$\boldsymbol{i}_m$	Motor current space vector
i_{ma}	Motor current a-phase
i_{mb}	Motor current b-phase
i_{md}	Motor current d-axis
i_{mq}	Motor current q-axis
i_{mu}	Motor current u-phase
i_{mv}	Motor current v-phase
i_{mw}	Motor current w-phase
$\boldsymbol{i}_s$	Suspension current space vector
i_{sa}	Suspension current a-phase
i_{sb}	Suspension current b-phase
i_{sd}	Suspension current d-axis
i_{sq}	Suspension current q-axis
i_{su}	Suspension current u-phase
i_{sv}	Suspension current v-phase
i_{sw}	Suspension current w-phase
$\boldsymbol{I}$	Identity matrix
j	Rotating reference j-axis
$\boldsymbol{J}$	Orthogonal rotation matrix
J_{tot}	Moment of inertia
K_i	General integral gain
$\boldsymbol{K}_{im}$	Motor integral gain matrix
$\boldsymbol{K}_{is}$	Suspension integral gain matrix
K_p	General proportional gain

$\boldsymbol{K}_{pm}$	Motor proportional gain matrix
$\boldsymbol{K}_{ps}$	Suspension proportional gain matrix
L	General inductance
$\boldsymbol{L}$	General inductance matrix
$\boldsymbol{L}_m$	Motor inductance matrix
L_d	Motor d-axis inductance
L_q	Motor q-axis inductance
$\boldsymbol{L}_s$	Suspension inductance matrix
L_s	Suspension inductance
$\boldsymbol{M}$	Mutual inductance matrix
M'_d	Suspension force constant d-axis
M'_q	Suspension force constant q-axis
p	Pair of poles
R	General resistance
R_m	Motor resistance
R_s	Suspension resistance
T_e	Electromagnetic torque
T_l	Load torque
$\boldsymbol{u}$	General voltage
$\boldsymbol{u}'$	New general voltage
$\boldsymbol{u}_m$	Motor voltage space vector
$\boldsymbol{u}_s$	Suspension voltage space vector
x	Stationary reference x-axis
y	Stationary reference y-axis
α_c	General current control bandwidth
α_{cm}	Motor current control bandwidth
α_{cs}	Suspension current control bandwidth
α_s	Speed closed-loop system bandwidth
θ	Phase angle between current and terminal voltage
τ_c	General closed-loop electrical time constant
ϕ	Mechanical angle of the rotor between i- and x-axis
ϕ_{elec}	Electrical angle of the rotor
$\boldsymbol{\psi}_m$	Motor winding flux linkage space vector
ψ_{md}	Motor flux linkage d-axis winding
ψ_{mq}	Motor flux linkage q-axis winding
$\boldsymbol{\psi}_{pm}$	Permanent magnets flux linkage vector
ψ_{pm}	Permanent magnets flux linkage
$\boldsymbol{\psi}'_{pm}$	Suspension force constant vector
ψ'_{pm}	Suspension force constant
$\boldsymbol{\psi}_s$	Suspension winding flux linkage space vector
ψ_{sd}	Suspension flux linkage d-axis winding
ψ_{sq}	Suspension flux linkage q-axis winding
ω	Mechanical angular speed of the rotor

Superscripts

x^s Stator reference frame

Subscripts

ref Reference value

Abbreviations

AC	Alternating current
BSyRM	Bearingless synchronous reluctance motor
PI	Proportional-integral
PMSM	Permanent-magnet synchronous motor
SyRM	Synchronous reluctance motor

1 Introduction

Synchronous reluctance motors (SyRMs) have recently become an interesting alternative to other AC machines in variable-speed drives [1]. One of the main reasons is that they drive well a very wide range of applications. Some of the characteristics that make modern transverse-laminated SyRMs so attractive are [2, 3]:

1. Simple and robust mechanical structure.
2. High efficiency and temperature capacity. The absence of the rotor winding results in a higher efficiency and temperature capacity compared to the induction motor.
3. Low production cost. The absence of magnets in the rotor results in production savings compared to the permanent-magnet synchronous motor (PMSM) production.
4. Low vibration, noise and torque ripple. These magnitudes are lower in SyRMs compared to the switched reluctance motor.
5. High saliency ratio.

Although SyRMs have some advantages, there are still issues to be considered. One of the problems is the modelling of the magnetic saturation. Other important problem is that in high-speed applications, the losses of the mechanical bearings become significant. Lubrication oil and bearings should be replaced periodically. In some environments, it is not easy to replace components, or the lubrication oil cannot be used. In order to avoid these losses, active magnetic bearings can be used, reducing the maintenance and removing the lubrication needs. However, there still remain some problems in magnetic bearings. One of these problems is that magnetic bearings require a large area. If the shaft length is increased to provide enough space to magnetic bearings, the critical rotating speed of the shaft decreases. To avoid complicated control of a flexible shaft, the length of the shaft has to be as short as possible. [1, 4–9]

One of the solutions, to reduce the axial shaft length of high speed motors with magnetic bearings, is to magnetically combine a motor with magnetic bearings. Hence bearingless synchronous reluctance motors (BSyRMs), are magnetically combined electric machines with magnetic bearings. Some of the most important advantages due to this integration are [1, 4–11]:

- Compactness. In BSyRMs the shaft length is shorter. Thus bearingless motors can achieve higher speed than motors with conventional magnetic bearings, resulting in a more stable operation.

- High power. The length of the rotor can be effectively used to produce both the torque and the radial magnetic force. Hence the electrical power required for shaft levitation can be reduced because the magnetizing flux of the motor is utilized as a bias for the radial force generation.
- Low cost. The number of wires and inverters is lower.

Therefore BSyRM can be applied to many emerging applications, which require a compact size, high-power, high reliability, long life, or wide temperature range together with operation at high speeds or active vibration control.

Other types of bearingless motors, which have integrated magnetic bearings with electric motors, have been proposed and developed actively in the last decades. Some of these motors are bearingless induction motors, bearingless switched reluctance motors or bearingless permanent-magnet synchronous motors. These motors have been developed in order to fulfil the need of high-power and high-speed AC drives together with an enormous reduction in size and weight.

The machine used in this final project, is a BSyRM with 4-pole motor winding for torque production, and 2-pole suspension winding for radial force generation. The BSyRM is a special case of the PMSM. Therefore, general PMSM equations have been presented for the machine dynamic model, in order to study a more general case applicable to a wide range of machines [9]. These equations have been specified for the BSyRM considering different assumptions.

The main goal of this final project is to describe the BSyRMs operation principles, to obtain the dynamic model equations and to implement the model of the machine in Simulink. An additional goal is to control the motor operation through the vector control developed. Hence, this final project will be focused in the development of the dynamic model and the vector control of BSyRMs.

In this final project, the description and operating principles of BSyRMs are explained in Section 2. Subsequent the equations of the dynamic model are obtained together with the assumptions and parameters used. The description of the vector control employed for controlling the machine is defined in Section 3. Section 4 includes the implementation of both the machine model and the vector control model of the BSyRM. Finally, Section 5 shows the simulations results obtained testing the Matlab/Simulink model developed, and Section 6 includes the final conclusions of this final project.

2 Bearingless synchronous reluctance motor drive

2.1 Bearingless synchronous reluctance motors

Figure 1 shows four main concepts that can be used to understand bearingless synchronous reluctance motors. These concepts are: magnetic bearings, motor windings, suspension windings and vector control theory.

Currently, mechanical bearings represent most of the maintenance requirements in an industrial drive. As it was mentioned in Section 1, the use of magnetic bearings reduces these losses, but still presents some problems. Thus the advantages of using bearingless motors can enlarge the possible application areas of motor drives.

One of the novelties that BSyRMs introduce, is the existence of extra windings in addition to the conventional motor windings. These additional windings, called suspension windings, are the responsible of radial force generation, while the motor windings produce the torque. In this point, it is important to mention the vector control theory. Bearingless motors often take advantage of the magnetic field set up by the motor winding currents. Controllers based on vector control theory provide instantaneous torque regulation as well as revolving magnetic field regulation. Hence the rotational position and amplitude of the magnetic field can be regulated. Based on the angular position and the amplitude of the motor magnetic field, radial forces are generated by generating additional magnetic fields using the suspension winding current. Therefore, it can be said that bearingless technology stands on vector control theory. [10]

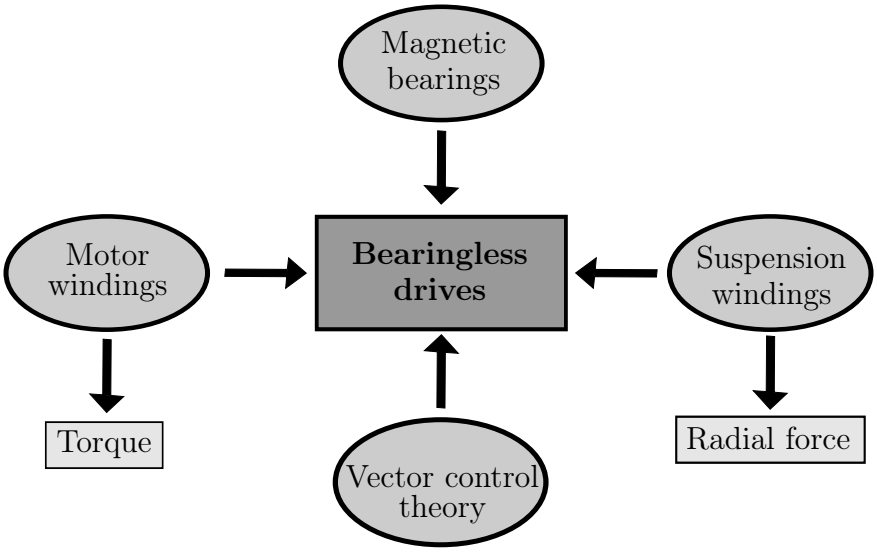

Figure 1: Bearingless technology.

2.1.1 General aspects

The machine studied in this final project is a "4-pole and 2-pole winding" BSyRM. The 4-pole refers to the motor winding set for torque production, while the 2-pole refers to the suspension winding set for radial force generation.

Figure 2 shows the cross section of a 2-phase ac bearingless machine. Typically, both the rotor and the stator are constructed from laminated silicon steel. The stator contains the slots for both n-pole motor windings and $(n \pm 2)$-pole suspension windings. The 4-pole motor windings *ma*-*mb* and 2-pole suspension windings *sa*-*sb* can be observed in Figure 2. The internal rotor has four salient poles and the field-winding conductors m are arranged so that 4-pole magnetization is produced. Two perpendicular axes, x and y, are set to the stator according to the magnetization direction of the a-phase. The i- and j-axes are aligned on the magnetic poles. These i- and j-axes are fixed to the rotor so that they rotate with rotor rotation. The radial position relationships between the i- and j-axes and the x- and y-axes are defined by

$$\begin{bmatrix} i \\ j \end{bmatrix} = \begin{bmatrix} \cos\phi & \sin\phi \\ -\sin\phi & \cos\phi \end{bmatrix} \begin{bmatrix} x \\ y \end{bmatrix} \tag{1}$$

where the rotor angular position is defined by the angle ϕ. [10, 11]

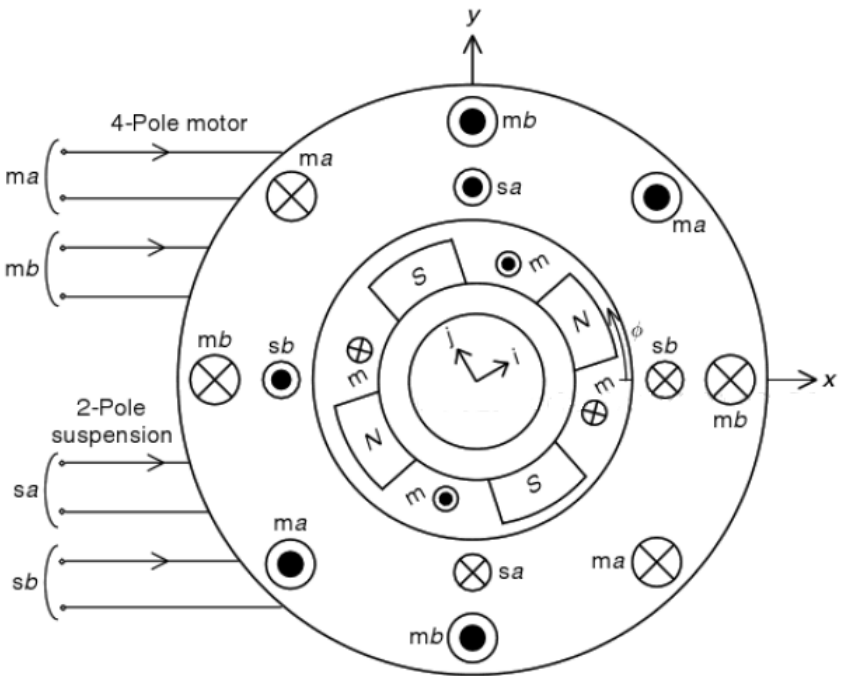

Figure 2: 2-Phase ac bearingless machine. [10]

Figure 3 shows the cross section of a 4-pole BSyRM. Only the u-phase motor and suspension windings are shown in order to simplify the figure. The v- and w-phases are located on the one-third and two-thirds rotational positions of the u-phase with electrical angle, respectively. The stator has a cylindrical inner surface and the stator windings have general sinusoidal distribution. Because the rotor has salient poles, reluctance torque is produced when the 4-pole motor winding is excited and there is a phase angle (rotational torque is generated by an interaction of the revolving magnetic field and the component of MMF that is perpendicular to the field on the d-q axes). In order to produce torque effectively with low current, the airgap should be designed to be as small as possible and a high saliency ratio is necessary to achieve high torque and power-factor. [10, 11]

The BSyRMs have a considerable force-displacement factor and require unbalanced magnetic pull compensation. The unbalanced magnetic pull should not be neglected in order to realize stable and robust magnetic suspension. Due to the small airgap of this type of machines, the inductances vary significantly with the rotor displacement. Since the inductances increase with rotor displacement, the generated unbalanced magnetic pull is in the displaced direction (where the airgap flux is most concentrated), so that the displacement-originated force is proportional to the radial displacement. [10]

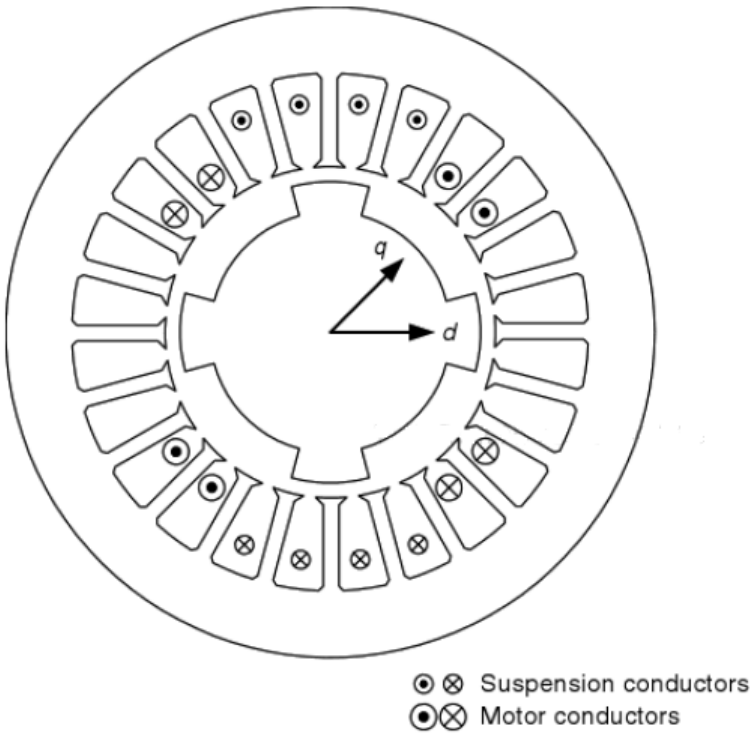

Figure 3: Rotor and stator of a synchronous reluctance bearingless motor. [10]

2.1.2 Mechanical structure

Bearingless motors present several typical structures. Some of these structures are described below. Other relevant structures can be found in the book written by Chiba et al. [10]

Figure 4 shows two-axis active magnetic suspension. This structure is appropriate for machines with a vertical shaft. In Figure 4, the shaft is introduced into a rotor core. At the bottom of the shaft, a pivot bearing is located for axial and radial positioning of the shaft end. Two-axis magnetic suspension is realized by magnetic forces between the rotor and the stator. [10]

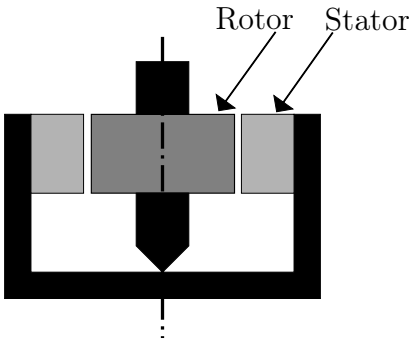

Figure 4: Two-axis active suspension: pivot bearing at the bottom.

Figure 5 shows cross-section of five-axis active suspension. Two bearingless units are needed in order to generate radial forces in four axes. A thrust magnetic bearing is also required for active axial positioning on the fifth axis. When axial force is low or precise axial positioning is not required, the thrust magnetic bearing is not necessary. In Figure 5, it can be observed that the shaft is inserted into two rotors. These rotors are acting in tandem. The rotor and the shaft are rotating inside two stator cores. [10]

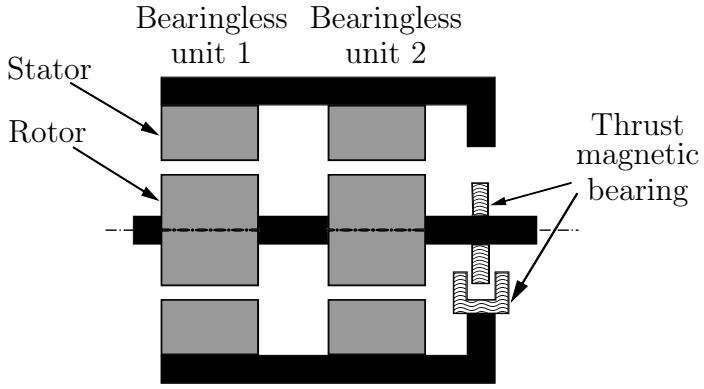

Figure 5: Five-axis active suspension variation: inner rotor.

2.1.3 Principles of radial force generation

In both radial magnetic bearing and bearingless motors, rotor radial force is generated by an unbalanced magnetic field; i.e., the rotor radial force is generated by the difference of radial forces between the magnetic poles.

Figure 6 shows the principles of rotor radial force generation. A rotating shaft is surrounded by the stator core. There are strong magnetic attractive forces under the four magnetic poles between the rotor and the stator cores. In Figure 6 (a), the four magnetic poles have equal flux density and thus equal attractive force magnitudes. Hence, a vector sum of the four radial forces is zero. However, in Figure 6 (b), one north pole is stronger than the other three poles so that the net attractive force is strong. Therefore the unbalanced airgap flux density distribution results in radial magnetic force acting in the rotor. The attractive force is an inherently unstable force as it is stronger if the motor moves in the force direction. [10, 11]

Figures 7, 8 and 9 show how the radial force is generated in different directions. When the rotor is centered and not radial forces are needed, the 2-pole winding currents are zero. If radial force is required, the suspension currents are no longer zero. In Figure 7, only the 4-pole conductors (4a) are excited. Hence the flux distribution is symmetrical, so the amplitudes of the attractive radial magnetic forces between the rotor poles and the stator iron are the same. The directions are equally distributed so that the sum of radial force acting on the rotor is zero. [1,4,5,7,8,10,11]

In Figures 8 and 9, the 2-pole suspension windings (2a-2b) are also excited together with the 4-pole conductors (4a). Thus the flux density is increased or decreased depending on the direction of the 4-pole and 2-pole fluxes. If the direction of the 4-

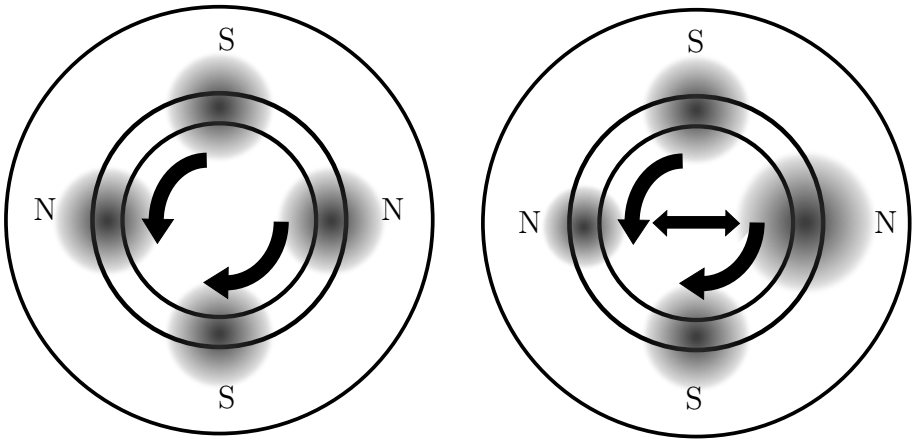

Figure 6: Radial force generation by unbalanced airgap flux density: (a) balanced airgap flux density; (b) unbalanced airgap flux density.

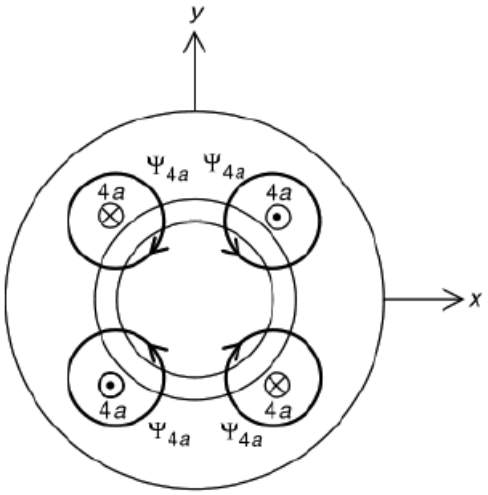

Figure 7: Principles of radial force generation: 4-pole symmetrical flux. [10]

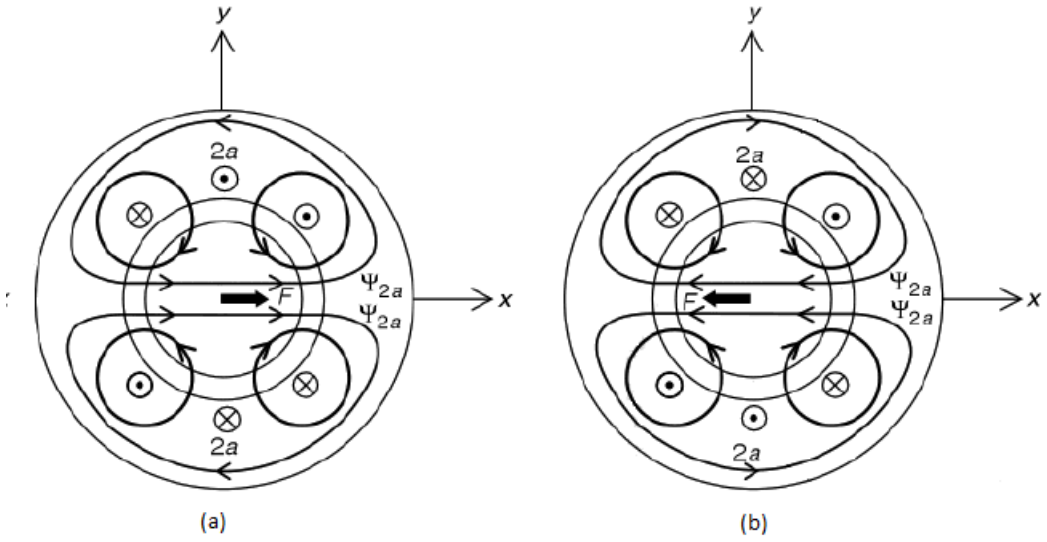

Figure 8: Principles of radial force generation: (a) x-direction radial force; (b) negative x-direction radial force. [10]

pole and 2-pole fluxes is the same the flux density is increased, while if the direction is the opposite the flux density is decreased. Therefore, there is a flux density imbalance, and a radial force results in the x- or y-axis. The vector sum of these two perpendicular radial forces can produce a radial force in any desired direction and with any amplitude. This compositional suspension force depends on torque-load conditions. The polarity of the current will decide the direction of the force. The radial force increases as the current value in conductors 2a-2b increases. [1, 4, 5, 7, 8, 10, 11]

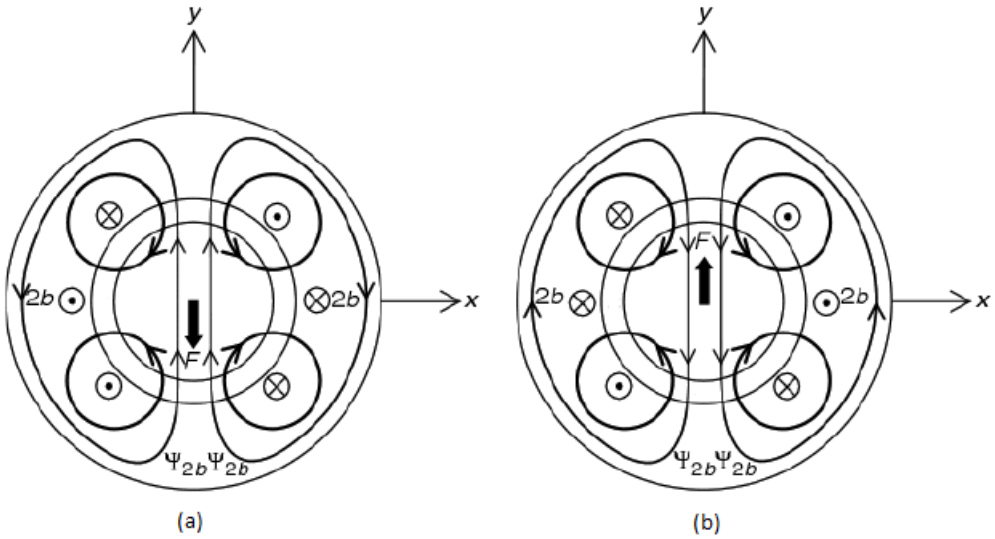

Figure 9: Principles of radial force generation: (a) negative y-direction radial force; (b) y-direction radial force. [10]

This relation is true only at no torque load. Under torque-load condition, the torque component current also generates the radial force and interferences in suspension force production appear. The radial force generated by the torque component is perpendicular to that generated by magnetizing current component. Hence the torque component flux causes cross couplings in radial force production. In order to cancel the cross couplings and achieve a stable rotor position control, a decoupling compensator is needed in the position control system. [1, 6, 11]

2.2 Space vectors

Vector control theory uses different reference frame transformations. One of these transformations is between 3-phase and 2-phase coordinate systems. This transformation for the current space vector is defined by

$$\boldsymbol{i}_m^s = \begin{bmatrix} i_{ma} \\ i_{mb} \end{bmatrix} = \frac{2}{3} \begin{bmatrix} 1 & -1/2 & -1/2 \\ 0 & \sqrt{3}/2 & -\sqrt{3}/2 \end{bmatrix} \begin{bmatrix} i_{mu} \\ i_{mv} \\ i_{mw} \end{bmatrix} \tag{2}$$

where $\boldsymbol{i}_m^s$ is the motor current space vector; i_{ma}, i_{mb} are the 2-phase motor currents and i_{mu}, i_{mv}, i_{mw} are the 3-phase motor currents, all of them in stationary references.

A similar expression is shown for suspension windings

$$\boldsymbol{i}_s^s = \begin{bmatrix} i_{sa} \\ i_{sb} \end{bmatrix} = \frac{2}{3} \begin{bmatrix} 1 & -1/2 & -1/2 \\ 0 & \sqrt{3}/2 & -\sqrt{3}/2 \end{bmatrix} \begin{bmatrix} i_{su} \\ i_{sv} \\ i_{sw} \end{bmatrix} \tag{3}$$

where the suspension variables are analogous to the ones of the motor.

Another type of transformation is between stationary/rotating (ab/dq) reference systems. This transformation applied to the motor current space vector can be carried out using the following matrix:

$$\boldsymbol{i}_m = \begin{bmatrix} i_{md} \\ i_{mq} \end{bmatrix} = \begin{bmatrix} \cos 2\phi & \sin 2\phi \\ -\sin 2\phi & \cos 2\phi \end{bmatrix} \begin{bmatrix} i_{ma} \\ i_{mb} \end{bmatrix} \tag{4}$$

where $\boldsymbol{i}_m$ is the motor current space vector in rotating coordinates and i_{md}, i_{mq} are the 2-phase motor currents in rotating reference system (d- and q-axis). A similar expression is used for suspension windings

$$\boldsymbol{i}_s = \begin{bmatrix} i_{sd} \\ i_{sq} \end{bmatrix} = \begin{bmatrix} \cos \phi & \sin \phi \\ -\sin \phi & \cos \phi \end{bmatrix} \begin{bmatrix} i_{sa} \\ i_{sb} \end{bmatrix} \tag{5}$$

It is necessary to distinguish between motor windings and suspension windings transformations, as the number of poles varies and therefore the angle used.

The motor and suspension windings transformations defined in the above expressions (4) and (5), can be also expressed using the following equations:

$$e^{\boldsymbol{J}2\phi} = \cos(2\phi)\boldsymbol{I} + \sin(2\phi)\boldsymbol{J} \tag{6}$$

$$e^{\boldsymbol{J}\phi} = \cos(\phi)\boldsymbol{I} + \sin(\phi)\boldsymbol{J} \tag{7}$$

where the identity matrix and the orthogonal rotation matrix are defined as

$$\boldsymbol{I} = \begin{bmatrix} 1 & 0 \\ 0 & 1 \end{bmatrix} \qquad \boldsymbol{J} = \begin{bmatrix} 0 & -1 \\ 1 & 0 \end{bmatrix}$$

respectively.

2.3 Dynamic model equations

To implement the dynamic model of the bearingless synchronous reluctance machine the following equations presented are needed. The equations are based on [8, 10, 12]. These expressions will help to understand the operation and performance of BSyRMs.

2.3.1 Voltage equations

The motor and suspension voltage equations in the stator reference frame (denoted by superscript s) are

$$\frac{d\boldsymbol{\psi}_m^s}{dt} = \boldsymbol{u}_m^s - R_m \boldsymbol{i}_m^s \tag{8}$$

$$\frac{d\boldsymbol{\psi}_s^s}{dt} = \boldsymbol{u}_s^s - R_s \boldsymbol{i}_s^s \tag{9}$$

where $\boldsymbol{\psi}_m$, $\boldsymbol{\psi}_s$ are the flux linkage space vectors; $\boldsymbol{u}_m$, $\boldsymbol{u}_s$ are the voltage space vectors; R_m, R_s are the resistances and $\boldsymbol{i}_m$, $\boldsymbol{i}_s$ are the current space vectors of the motor and suspension windings, respectively, in each case.

In order to use rotating coordinates instead of stator coordinates, the following transformations are needed:

$$\boldsymbol{\psi}_m^s = \boldsymbol{\psi}_m e^{\boldsymbol{J}2\phi} \tag{10}$$

$$\boldsymbol{\psi}_s^s = \boldsymbol{\psi}_s e^{\boldsymbol{J}\phi} \tag{11}$$

The angular speed of the rotor is defined by

$$\omega = \frac{d\phi}{dt} \tag{12}$$

where ϕ is the mechanical angle of the rotor between i-axis and x-axis as it was mentioned previously.

Transforming (8) and (9) to the synchronous reference frame gives

$$\frac{d\boldsymbol{\psi}_m}{dt} = \boldsymbol{u}_m - R_m\boldsymbol{i}_m - \boldsymbol{J}2\omega\boldsymbol{\psi}_m \tag{13}$$

$$\frac{d\boldsymbol{\psi}_s}{dt} = \boldsymbol{u}_s - R_s\boldsymbol{i}_s - \boldsymbol{J}\omega\boldsymbol{\psi}_s \tag{14}$$

These expressions (13) and (14) will be used for the implementation of the voltage equations. The use of the equations in rotating coordinates is because if stationary coordinates are employed, the flux equations would be much more complicated.

2.3.2 Flux equations

The relationships between flux linkage and winding currents can be expressed in a matrix form

$$\begin{bmatrix} \psi_{md} \\ \psi_{mq} \\ \psi_{sd} \\ \psi_{sq} \end{bmatrix} = \begin{bmatrix} L_d & 0 & M'_d i & -M'_d j \\ 0 & L_q & M'_q j & M'_q i \\ M'_d i & M'_q j & L_s & 0 \\ -M'_d j & M'_q i & 0 & L_s \end{bmatrix} \begin{bmatrix} i_{md} \\ i_{mq} \\ i_{sd} \\ i_{sq} \end{bmatrix} + \begin{bmatrix} \psi_{pm} \\ 0 \\ \psi'_{pm} i \\ -\psi'_{pm} j \end{bmatrix} \tag{15}$$

where ψ_{md}, ψ_{mq}, ψ_{sd}, ψ_{sq} and i_{md}, i_{mq}, i_{sd}, i_{sq} are, respectively, flux linkages and currents of the motor and suspension d- and q-axis windings; L_d, L_q and L_s are motor d- and q-axis inductances and suspension inductance; ψ_{pm} is the permanent magnets flux linkage and ψ'_{pm} (Wb/m), M'_d (H/m) and M'_q (H/m) are the suspension force constants.

The expression (15) can be also expressed in vector form

$$\boldsymbol{\psi}_m = \boldsymbol{L}_m\boldsymbol{i}_m + \boldsymbol{M}\boldsymbol{i}_s + \boldsymbol{\psi}_{pm} \tag{16}$$

$$\boldsymbol{\psi}_s = \boldsymbol{M}^T\boldsymbol{i}_m + \boldsymbol{L}_s\boldsymbol{i}_s + \boldsymbol{\psi}'_{pm} \tag{17}$$

where $\boldsymbol{L}_m$, $\boldsymbol{L}_s$ are the motor and suspension inductance matrices, $\boldsymbol{M}$ is the mutual inductance matrix and $\boldsymbol{\psi}_{pm}$ and $\boldsymbol{\psi}'_{pm}$ are the permanent magnets flux linkage and suspension force constants vectors, respectively.

The definitions of the matrices mentioned above are

$$\boldsymbol{L}_m = \begin{bmatrix} L_d & 0 \\ 0 & L_q \end{bmatrix} \qquad \boldsymbol{L}_s = \begin{bmatrix} L_s & 0 \\ 0 & L_s \end{bmatrix} \qquad \boldsymbol{M} = \begin{bmatrix} M'_d i & -M'_d j \\ M'_q j & M'_q i \end{bmatrix}$$

$$\boldsymbol{\psi}_{pm} = \begin{bmatrix} \psi_{pm} \\ 0 \end{bmatrix} \qquad \boldsymbol{\psi}'_{pm} = \begin{bmatrix} \psi'_{pm} i \\ -\psi'_{pm} j \end{bmatrix}$$

2.3.3 Torque and motion equations

The electromagnetic torque of the bearingless synchronous reluctance machine can be written as:

$$T_e = 3[(L_d - L_q) i_{md} i_{mq} + \psi_{pm} i_{mq}] \tag{18}$$

The number 3 comes from $\frac{3}{2}p$, where p is the number of pair of poles of the motor windings. In the studied machine, $p = 2$. From (18) it is seen that the torque can be controlled with both d-axis and q-axis motor winding currents.

The mechanical dynamics are governed by the equation of motion

$$\frac{d\omega}{dt} = \frac{1}{J_{tot}}(T_e - T_l) \tag{19}$$

where J_{tot} is the moment of inertia and T_l is the load torque. The rotational speed of the shaft is controlled by the motor torque and described by (19). Mechanical dynamics related to radial position are omitted in this final project.

2.3.4 Suspension force equations

The BSyRM produces a suspension force by the superposition of the 4-pole motor flux and the 2-pole suspension flux

$$\begin{bmatrix} F_i \\ F_j \end{bmatrix} = \begin{bmatrix} M'_d i_{md} + \psi'_{pm} & M'_q i_{mq} \\ M'_q i_{mq} & -M'_d i_{md} - \psi'_{pm} \end{bmatrix} \begin{bmatrix} i_{sd} \\ i_{sq} \end{bmatrix} \tag{20}$$

The i- and j-axis suspension forces, F_i and F_j, are proportional to suspension currents, i_{sd} and i_{sq}, and to coefficients $M'_d i_{md} + \psi'_{pm}$ and $M'_q i_{mq}$, as it is shown in the

equation (20). The variables ψ'_{pm}, $M'_d i_{md}$ and $M'_q i_{mq}$ are the corresponding derivatives of the permanent magnets flux linkage and d- and q-axis winding flux linkages with respect to the radial rotor displacement. Thus, suspension force characteristics of bearingless motors can be determined using the suspension force constants ψ'_{pm}, M'_d and M'_q.

To modify the reference frame, some transformations should be completed

$$\begin{bmatrix} F_x \\ F_y \end{bmatrix} = \begin{bmatrix} \cos\phi & -\sin\phi \\ \sin\phi & \cos\phi \end{bmatrix} \begin{bmatrix} F_i \\ F_j \end{bmatrix} \tag{21}$$

$$\begin{bmatrix} i_{sd} \\ i_{sq} \end{bmatrix} = \begin{bmatrix} \cos\phi & \sin\phi \\ -\sin\phi & \cos\phi \end{bmatrix} \begin{bmatrix} i_{sa} \\ i_{sb} \end{bmatrix} \tag{22}$$

where the subscripts x, y refer to stationary reference and i, j refer to rotating reference system.

Applying the transformations (21) and (22) to the initial equation (20), it is obtained

$$\begin{bmatrix} F_x \\ F_y \end{bmatrix} = \begin{bmatrix} M'_d i_{md} + \psi'_{pm} & -M'_q i_{mq} \\ M'_q i_{mq} & M'_d i_{md} + \psi'_{pm} \end{bmatrix} \begin{bmatrix} \cos 2\phi & \sin 2\phi \\ \sin 2\phi & -\cos 2\phi \end{bmatrix} \begin{bmatrix} i_{sa} \\ i_{sb} \end{bmatrix} \tag{23}$$

This matrix equation (23) shows the relationship between the suspension forces in stationary coordinates as a function of the suspension winding currents. Therefore the radial forces, F_x and F_y, can be regulated using the suspension currents i_{sa} and i_{sb}. The magnitude of the force is a function of the rotor angular position ϕ and the suspension force constants which includes motor currents i_{md} and i_{mq}. Thus the suspension currents must be regulated in accordance with (23) in order to produce the required radial force.

2.4 Operating principle

Figure 10 shows a SyRM phasor diagram. Different variables are represented in the figure. The motor terminal voltage $\boldsymbol{u}_m$ comes from the steady state of the equation (13) and it is defined by

$$\boldsymbol{u}_m = \boldsymbol{e}_m + R_m \boldsymbol{i}_m \tag{24}$$

where the back-EMF $\boldsymbol{e}_m$ corresponds to

$$\boldsymbol{e}_m = \boldsymbol{J} 2\omega \boldsymbol{\psi}_m \tag{25}$$

As it is known, BSyRMs do not have permanent magnets. Hence, d-axis excitation is provided only by the d-axis component of the motor winding current. Depending on the saliency of the rotor, the d-axis inductance L_d should be much higher than q-axis inductance L_q. The ratio of L_d/L_q is defined as the saliency ratio.

As it can be observed, in Figure 3, the motor d-axis current i_{md} is equal to the motor q-axis current i_{mq}. The saliency ratio $L_d/L_q = 3$. A ratio of 3 is typical for the type of rotor shown in Figure 3. In the manufacture of modern transverse-laminated SyRMs, a much higher saliency ratio is possible. Since d-axis current is required for excitation, the phase angle θ between current and terminal voltage is rather large. Hence, typical SyRMs do not have high power-factor [10]. It is possible to increase the saliency ratio and the power-factor by some modifications of the rotor; e.g. a high saliency ratio can be obtained with flux barriers in the rotor.

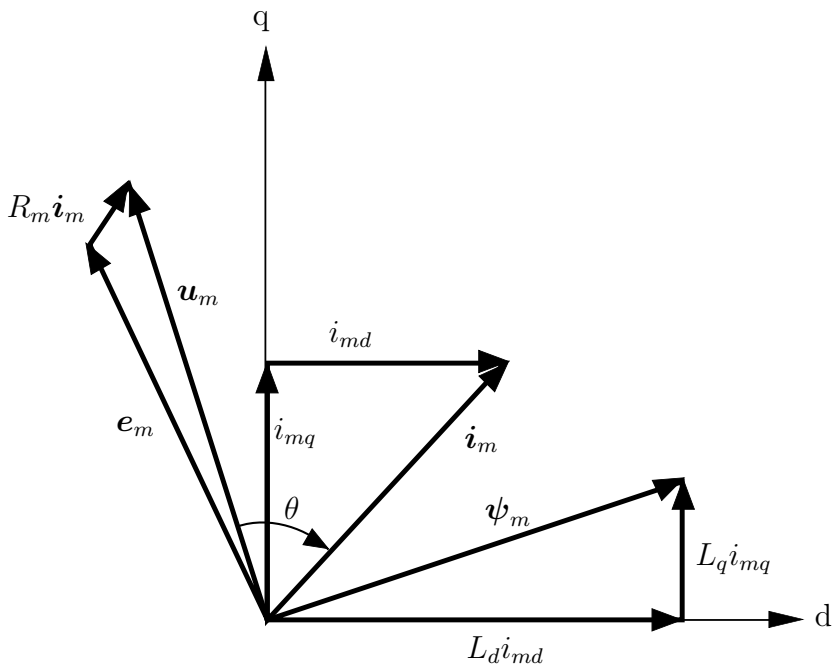

Figure 10: Phasor diagram.

2.5 Parameters and assumptions

The choice of the BSyRM parameters used for testing the Simulink model, has been based on the book written by Chiba et al. [10] and on [6]. Different methods of electrical parameter identification are described on [13, 14].

In this final project, inductances L_d and L_q are considered to be constant, while in real case, the machine saturates and the inductances are not constant and vary as a function of motor currents (or fluxes) and the operation point [13, 15]. The values of the parameters L_d and L_q have been obtained using Figure 11. Figure 11 shows the measured d- and q-axis inductances for the motor windings with respect to the normalized rotor radial displacement. The values of L_d and L_q corresponding to no rotor radial displacement ($x_n = 0$) are used for simulating the operation of the motor. The relationship $L_d/L_q = 3$ mentioned in [10] for the type of rotor shown in Figure 3 has been also taken into account.

The decision of d- and q-axis suspension force constants values, M'_d and M'_q, has been carried out using Figure 12. It is important to say that radial force constants exhibit significant variations in accordance with the torque component current due to magnetic saturation. Nevertheless, they are considered constants in this study. Figure 12 shows different values of the radial force constants under magnetic saturation. In order to obtain the values of M'_d and M'_q needed for testing the model, an average of the values that are given in the graph is taken. The values of M'_d and M'_q obtained in [6] have been also considered and the magnitudes reflected, match up with the ones obtained in [10].

About ψ_{pm} and ψ'_{pm}, in BSyRMs these parameters are zero. The chosen value of $i_{md,ref}$, is one of the values used on the tests carried out in [10]. Table 1 includes the numerical values of the parameters that are used in the machine dynamic model.

Table 1: BSyRM parameters.

Parameter	**Symbol**	**Value**
Direct-axis inductance	L_d	1.75 mH
Quadrature-axis inductance	L_q	0.5 mH
Direct-axis suspension force constant	M'_d	3.1 H/m
Quadrature-axis suspension force constant	M'_q	0.6 H/m
Permanent magnets flux linkage	ψ_{pm}	0 Wb
Suspension force constant	ψ'_{pm}	0 Wb/m
Moment of inertia	J_{tot}	0.0001 kgm^2
Direct-axis motor reference current	$i_{md,ref}$	8 A

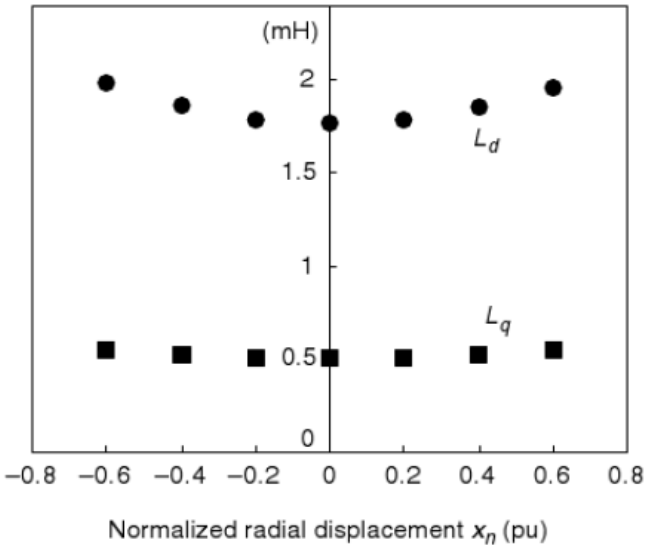

Figure 11: The d- and q-axis inductances of motor windings. [10]

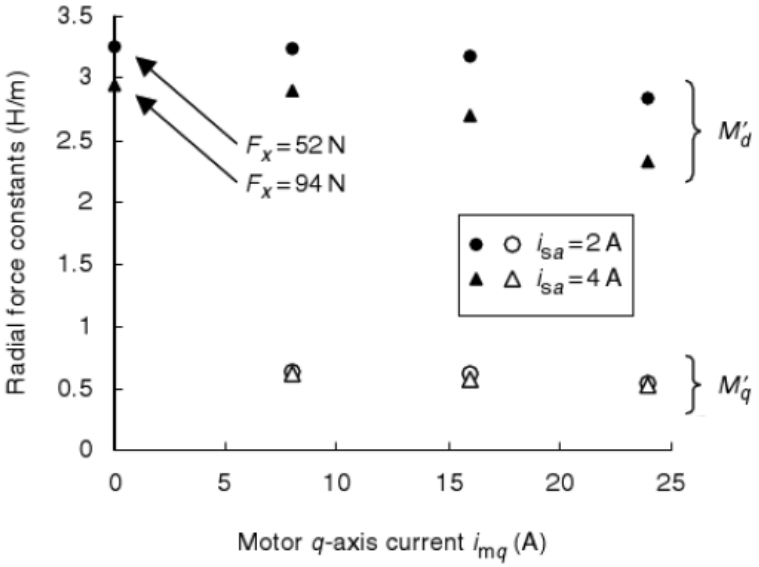

Figure 12: Radial force constants under magnetic saturation. [10]

3 Vector control

3.1 Vector control theory in bearingless motors

Vector control theory provides a control strategy to regulate the rotational torque as well as the radial force.

Bearingless synchronous reluctance motors need two different control systems, one for the motor and one for the suspension. The motor control is responsible for generating the revolving magnetic field for torque production and it regulates the instantaneous rotational torque. The suspension control generates additional magnetic fields and it regulates the radial force. Due to the radial force generated in BSyRMs, both control systems are linked and have dependent relationships.

The control that have been developed for this final project is a basic control. The controllers implemented are enough for the goal of this final project. This control will be improved in future studies.

3.1.1 Motor control system

The motor control is based on the relationships between torque and current. Torque and current are closely related. In AC motors, in order to control the torque, both the amplitude and phase angle of the currents have to be regulated.

Figure 13 shows a general idea of the motor control system. The *Angular speed controller* compares the speed with its reference signal, generating the corresponding reference torque. The reference of this electromagnetic torque is employed in the *Motor decoupling* to obtain the motor current reference. In the *Motor current controller* the motor current signal is compared with the motor current reference and finally the motor voltage vector is generated.

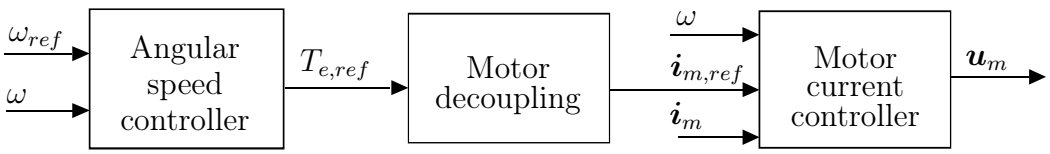

Figure 13: Motor control.

3.1.2 Suspension control system

The suspension control system is necessary for controlling the radial force generated by the suspension windings and keep the center of the shaft in the optimal position.

Figure 14 shows a general suspension control system. The *Suspension decoupling* block uses the motor current and the force reference for generating the suspension current reference. After this, the suspension current is compared with its reference and together with the speed the suspension voltage vector can be calculated through the *Suspension current controller*.

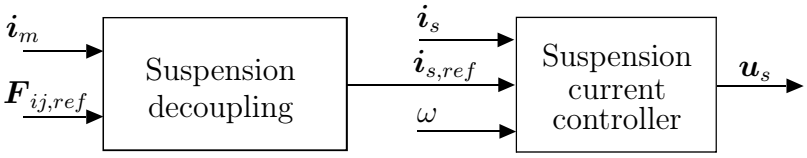

Figure 14: Suspension control.

3.2 Assumptions

For the implementation of the vector control of the BSyRM studied, some assumptions have to be taken into account.

Synchronous reluctance motors have no permanent magnet excitation. Hence as it has been said previously ψ_{pm} and ψ'_{pm} are zero. Thus the torque equation (18) and the suspension force equation (20) are simplified

$$T_e = 3(L_d - L_q) i_{md} i_{mq} \tag{26}$$

$$\begin{bmatrix} F_i \\ F_j \end{bmatrix} = \begin{bmatrix} M'_d i_{md} & M'_q i_{mq} \\ M'_q i_{mq} & -M'_d i_{md} \end{bmatrix} \begin{bmatrix} i_{sd} \\ i_{sq} \end{bmatrix} \tag{27}$$

Additionally, when designing current control, it is assumed $i = 0$ and $j = 0$. That means the shaft is considered centered and no mutual inductances are taken into account. Therefore the flux expressions (16) and (17) are reduced to

$$\boldsymbol{\psi}_m = \boldsymbol{L}_m \boldsymbol{i}_m \tag{28}$$

$$\boldsymbol{\psi}_s = \boldsymbol{L}_s \boldsymbol{i}_s \tag{29}$$

If (28) and (29) are substituted in the motor and suspension voltage equations, (13) and (14), the following expressions are obtained:

$$\boldsymbol{L}_m \frac{d\boldsymbol{i}_m}{dt} = \boldsymbol{u}_m - (R_m + \boldsymbol{J}2\omega\boldsymbol{L}_m)\boldsymbol{i}_m \tag{30}$$

$$\boldsymbol{L}_s \frac{d\boldsymbol{i}_s}{dt} = \boldsymbol{u}_s - (R_s + \boldsymbol{J}\omega\boldsymbol{L}_s)\boldsymbol{i}_s \tag{31}$$

The current control implementation of the motor and suspension will be based on these expressions.

3.3 Current controller

The general procedure that has to be followed for the implementation of the one-degree-of-freedom controller needed for the current controller is described below. This procedure is based on [16, 17].

First of all is necessary to obtain the transfer function G_e of the electrical dynamics from $\boldsymbol{u}'$ to $\boldsymbol{i}$. This procedure has to be done for the motor and suspension equations. Thus general expressions are used and later, the equations for each case are specified.

Start from a general equation similar to (30) and (31)

$$\boldsymbol{L}\frac{d\boldsymbol{i}}{dt} = \boldsymbol{u} - R\boldsymbol{i} - \boldsymbol{J}\omega\boldsymbol{L}\boldsymbol{i} \tag{32}$$

where $\boldsymbol{i}$ and $\boldsymbol{u}$ are the general current and voltage space vectors, R is the general resistance and $\boldsymbol{L}$ is the general inductance matrix.

A new voltage variable

$$\boldsymbol{u}' = \boldsymbol{u} - \boldsymbol{J}\omega\boldsymbol{L}\boldsymbol{i} \tag{33}$$

is defined to compensate the voltage $\boldsymbol{J}\omega\boldsymbol{L}\boldsymbol{i}$. Hence the system

$$\boldsymbol{L}\frac{d\boldsymbol{i}}{dt} = \boldsymbol{u}' - R\boldsymbol{i} \tag{34}$$

becomes linear and it is less complicated to design the current controller.

Applying the Laplace transform

$$s\boldsymbol{L}\boldsymbol{i}(s) = \boldsymbol{u}'(s) - R\boldsymbol{i}(s) \tag{35}$$

Finally the transfer function G_e from the new voltage variable, $\boldsymbol{u}'$, to the current, $\boldsymbol{i}$, is obtained

$$G_e(s) = \frac{1}{sL + R} \tag{36}$$

It is important to mention that the equation (36) has been written in scalar form to aid the understanding of the expressions. Nevertheless, the specific equations for the motor and suspension have a matrix form because of the inductance matrices.

The specific motor and suspension expressions for equation (32) are

$$\boldsymbol{L}_m \frac{d\boldsymbol{i}_m}{dt} = \boldsymbol{u}_m - R_m\boldsymbol{i}_m - \boldsymbol{J}2\omega\boldsymbol{L}_m\boldsymbol{i}_m \tag{37}$$

$$\boldsymbol{L}_s \frac{d\boldsymbol{i}_s}{dt} = \boldsymbol{u}_s - R_s\boldsymbol{i}_s - \boldsymbol{J}\omega\boldsymbol{L}_s\boldsymbol{i}_s \tag{38}$$

Therefore, the specific motor and suspension transfer functions from equation (36) in matrix form, as is was said previously, are

$$\boldsymbol{G}_{e,m}(s) = (s\boldsymbol{L}_m + R_m\boldsymbol{I})^{-1} \tag{39}$$

$$\boldsymbol{G}_{e,s}(s) = (s\boldsymbol{L}_s + R_s\boldsymbol{I})^{-1} \tag{40}$$

Once the transfer function has been calculated, the controller can be obtained. As previously, scalar variables are used in the explanation and matrix expressions are used in the specific final equations of the motor and suspension. A simple proportional-integral (PI) controller is sufficient for the propose of this final project

$$F_c(s) = K_p + \frac{K_i}{s} \tag{41}$$

where K_p and K_i are the general proportional and integral gains. Since good estimates of the motor parameters are known, they can be used to select the controller parameters K_p and K_i. The following procedure is employed to obtain these parameters.

The closed-loop transfer function from $\boldsymbol{i}_{ref}$ to $\boldsymbol{i}$ should be

$$G_{cc}(s) = \frac{\alpha_c}{s + \alpha_c} = \frac{1}{s\tau_c + 1} \tag{42}$$

$$\alpha_c = \frac{1}{\tau_c} \tag{43}$$

where α_c is the general current control bandwidth and τ_c is the general closed-loop electrical time constant.

Known that $G_{cc}(s)$ can be also expressed as

$$G_{cc}(s) = \frac{F_c(s)G_e(s)}{1 + F_c(s)G_e(s)} \tag{44}$$

$$F_c(s)G_e(s) = \frac{\alpha_c}{s} \tag{45}$$

the desired closed-loop system is obtained

$$F_c(s) = \frac{\alpha_c}{s}G_e^{-1}(s) = \frac{\alpha_c}{s}(sL + R) = \alpha_c L + \frac{\alpha_c R}{s} \tag{46}$$

That is,

$$K_p = \alpha_c L \tag{47}$$

$$K_i = \alpha_c R \tag{48}$$

If the equation (41) is specified for the motor and suspension cases, the PI-controllers

become

$$\boldsymbol{F}_{c,m}(s) = \boldsymbol{K}_{pm} + \frac{1}{s}\boldsymbol{K}_{im} \tag{49}$$

$$\boldsymbol{F}_{c,s}(s) = \boldsymbol{K}_{ps} + \frac{1}{s}\boldsymbol{K}_{is} \tag{50}$$

where $\boldsymbol{K}_{pm}$ and $\boldsymbol{K}_{im}$ are the proportional and integral motor gain matrices and $\boldsymbol{K}_{ps}$ and $\boldsymbol{K}_{is}$ are the proportional and integral suspension gain matrices.

From equations (47) and (48), the specific expressions for motor and suspension controller parameters are

$$\boldsymbol{K}_{pm} = \alpha_{cm}\boldsymbol{L}_m \tag{51}$$

$$\boldsymbol{K}_{im} = \alpha_{cm}R_m\boldsymbol{I} \tag{52}$$

$$\boldsymbol{K}_{ps} = \alpha_{cs}\boldsymbol{L}_s \tag{53}$$

$$\boldsymbol{K}_{is} = \alpha_{cs}R_s\boldsymbol{I} \tag{54}$$

where α_{cm} and α_{cs} are the motor and suspension current control closed-loop system bandwidth, respectively.

It is important to mention that $\boldsymbol{L}_m$ and $\boldsymbol{L}_s$ are matrices, but R_m and R_s are scalars. Hence when implementing the equations it is needed to multiply R_m and R_s by the identity matrix $\boldsymbol{I}$.

Figure 20 and Figure 21, included in Section 4.2, show the implementation in Simulink of these motor and current controllers, respectively.

3.4 Decoupling controller

The motor torque flux causes cross couplings in suspension force generation. Hence the BSyRM requires a decoupling controller between the motor torque current and the suspension force in order to realize the stable operation under torque-load conditions [6, 11]. A BSyRM includes motor and suspension windings. Thus two decoupling controllers are needed, one for the motor and one for the suspension.

The motor decoupling implementation is based on equation (26), used in the form

$$i_{mq} = \frac{T_e}{3(L_d - L_q)i_{md}} \tag{55}$$

so $i_{mq,ref}$ can be calculated and together with $i_{md,ref}$, the reference vector $\boldsymbol{i}_{m,ref}$ can be obtained.

The suspension decoupling includes the implementation of the equation (27) in the following form:

$$\begin{bmatrix} i_{sd} \\ i_{sq} \end{bmatrix} = \begin{bmatrix} M'_d i_{md} & M'_q i_{mq} \\ M'_q i_{mq} & -M'_d i_{md} \end{bmatrix}^{-1} \begin{bmatrix} F_i \\ F_j \end{bmatrix} \tag{56}$$

so once calculated i_{sd} and i_{sq}, the vector $\boldsymbol{i}_{s,ref}$ is obtained.

Figure A7 and Figure A8, included in Appendix A, show the implementation in Simulink of both decoupling controllers.

3.5 Parameters

Table 2 shows the closed-loop system bandwidth values, α_{cm}, α_{cs} and α_s that have been selected, where α_s is the speed closed-loop system bandwidth. The values of the integral and proportional motor and suspension gain matrices ($\boldsymbol{K}_{im}$, $\boldsymbol{K}_{is}$, $\boldsymbol{K}_{pm}$, $\boldsymbol{K}_{ps}$) have been calculated using the equations defined in Section 3.3. Substituting the machine parameters that have been described in Section 2.5 into the equations (51), (52), (53) and (54), these controller gain matrices are obtained. [13]

Table 2: Vector control parameters.

Parameter	**Symbol**	**Value**
Motor current-controller bandwidth	α_{cm}	100 rad/s
Suspension current-controller bandwidth	α_{cs}	1000 rad/s
Speed-controller bandwidth	α_s	10 rad/s

4 Simulink model

For the simulation of the operation of the bearingless synchronous reluctance motor, a Simulilnk model has been developed.

Figure 15 shows the main level of the model implemented in Matlab/Simulink. The *Vector control* block contains all the controllers needed for the motor and suspension control systems. The *BSyRM and mechanics* block includes the implementation of all the equations which describe the dynamic model of the BSyRM. As shown, both main blocks are linked and share inputs and outputs. Two reference inputs are used. The variable ω_{ref} is the angular speed reference of the rotor and $\boldsymbol{F}_{xy,ref}$ is the radial force reference vector, which includes x- and y-axis radial forces.

In the following sections, the blocks and the equations used in their development are described. The inner structure of some of the main blocks is shown. The Simulink blocks that are not detailed in this section can be found in the Appendix A.

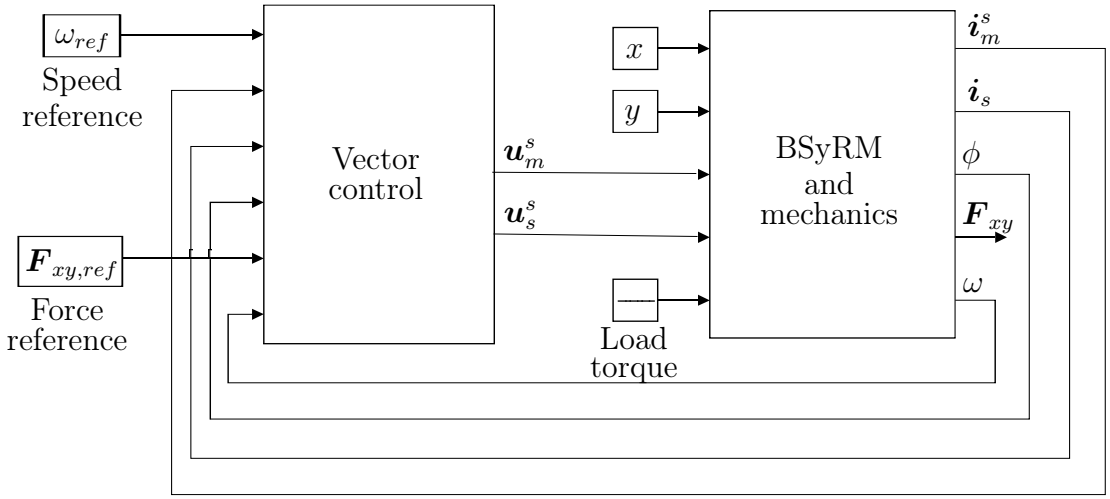

Figure 15: Simulink model.

4.1 Machine model

Figure 16 shows the dynamic model of the BSyRM that has been implemented. The model has five main blocks: *Voltage equations*, *Flux equations*, *Motion equation*, *Torque equation* and *Force equations*.

The inputs of the machine dynamic model are $\boldsymbol{u}_m^s$ and $\boldsymbol{u}_s^s$ that come from the *Vector control* block and T_l, x, y that are some of the inputs that can be modified in the

main level of the model. The outputs are $\boldsymbol{i}_m^s$, $\boldsymbol{i}_s^s$, $\boldsymbol{F}_{xy}$, ϕ and ω. As it is seen from Figure 16, inputs and outputs are in the stationary reference system and they have to be transformed into the rotating reference system before being used in the equations.

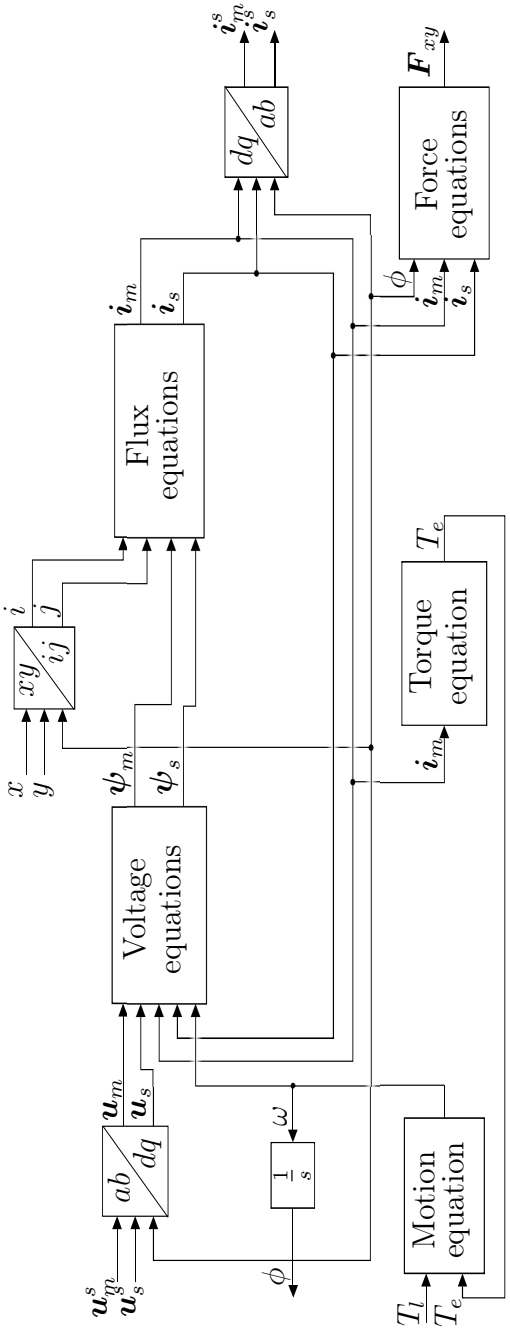

Figure 16: BSyRM and mechanics.

4.1.1 Voltage equations block

Figure 17 shows the voltage equations implementation. The top portion corresponds to the motor equation (13) and the bottom portion corresponds to the suspension equation (14).

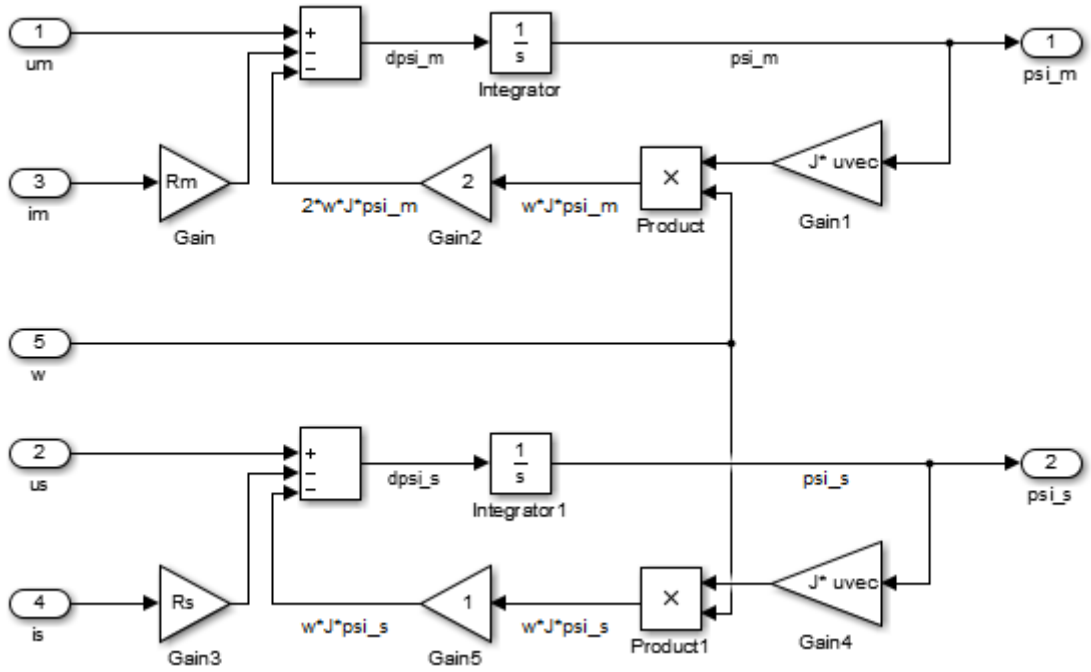

Figure 17: Voltage equations block.

It can be seen that the structure of both motor and suspension voltage equations implementation is analogous. There is a difference on the $Gain2$ and $Gain5$ values. In the motor $Gain2 = 2$ and in the suspension $Gain5 = 1$. This difference comes from the pair of poles of each winding. While the motor has 2-pair poles, the suspension has 1-pair poles. This value affects the electrical angle

$$\phi_{elec} = p\phi \tag{57}$$

so for the motor $\phi_{elec} = 2\phi$ and for the suspension $\phi_{elec} = 1\phi$.

4.1.2 Flux equations block

Flux equations implementation is shown in the Appendix A, Figure A2. In this case a MATLAB function has been used in order to implement the equation (15) and obtain the motor and suspension currents.

4.1.3 Torque and motion equations blocks

Torque equation block is shown in the Appendix A, Figure A3. For implementing the torque equation (18), a MATLAB function has been chosen.

Motion equation (19) is quite simple to implement and it is shown in the Appendix A, Figure A4. It has been build using common blocks from the Simulink library.

4.1.4 Force equations block

The implementation of the force equations is shown in Figure 18. For the design of this block, two equations have been used. On the bottom of the figure, the equation (20) is used to obtain the forces F_i and F_j, and on the top of the figure, the equation (21) is used to transform the forces from rotating to stationary references.

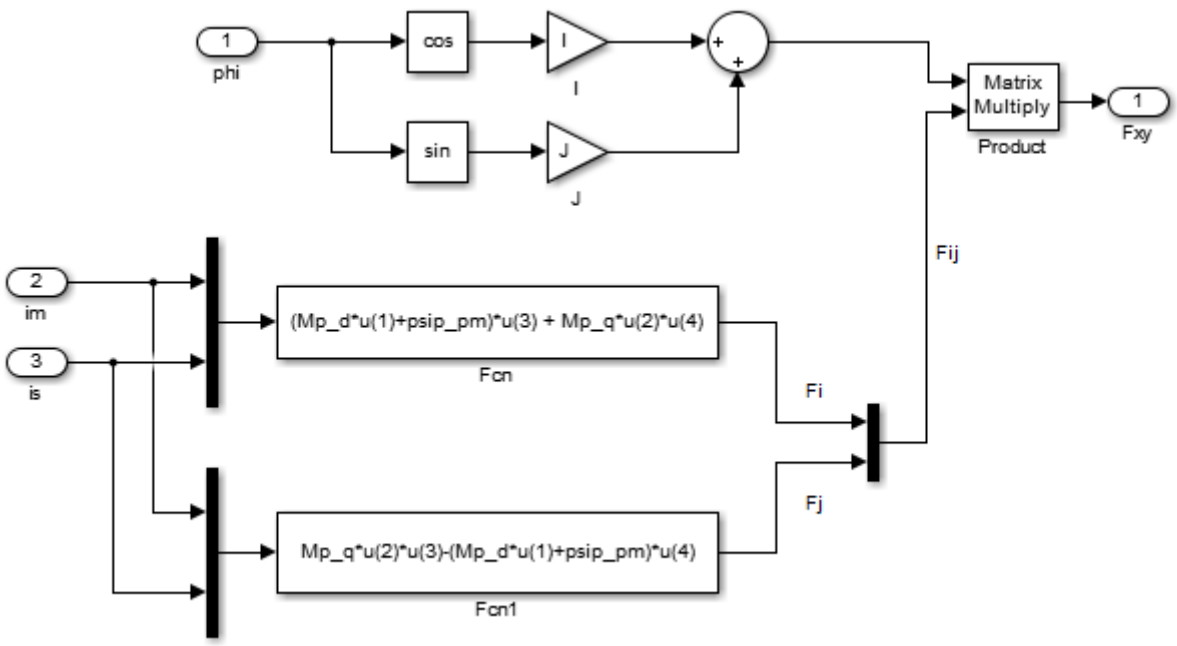

Figure 18: Force equations block

4.2 Vector control model

Figure 19 shows the vector control of the BSyRM that has been implemented. The control has five main blocks. Inside the vector control model it is necessary to dis-

tinguish between the motor control and the suspension control. The top portion corresponds to the motor control and it is composed of the *Angular speed controller*, *Motor decoupling* and *Motor current controller*. The suspension control is represented on the bottom portion and it is composed of the *Suspension decoupling* and the *Suspension current controller*.

There are inputs of the vector control that can be modified in the main level of the model as ω_{ref} and $\boldsymbol{F}_{xy,ref}$. Other inputs come from the *BSyRM and mechanics* block as $\boldsymbol{i}_m^s$, $\boldsymbol{i}_s^s$, ϕ and ω. The outputs are $\boldsymbol{u}_m^s$ and $\boldsymbol{u}_s^s$ and they go directly to the *BSyRM and mechanics* block. As it happened in the dynamic model of the machine, in the control inputs and outputs are in the stationary reference system and they have to be transformed into the rotating reference system.

4.2.1 Angular speed controller

A PI controller has been used for the control of the angular speed. Figure A6, included in Appendix A, shows the implementation of this speed control. The block includes two inputs ω_{ref} and ω that are compared. Depending on these inputs the torque reference, $T_{e,ref}$, is produced as output. This torque reference is used in the motor decoupling block, where the motor current reference, $\boldsymbol{i}_{m,ref}$, is generated.

4.2.2 Motor decoupling

The motor decoupling includes the implementation of the equation (55). This implementation can be found in the Appendix A, Figure A7. The d-axis motor current reference, $i_{md,ref}$, and the torque reference, $T_{e,ref}$, are taken as inputs. The value of $i_{md,ref}$ depends on the operation point chosen. Hence q-axis motor current reference, $i_{mq,ref}$, can be calculated, allowing to obtain the motor current reference vector $\boldsymbol{i}_{m,ref}$ as output.

4.2.3 Suspension decoupling

The suspension decoupling implementation can be found in Appendix A, Figure A8. The force vector $\boldsymbol{F}_{ij}$ includes i- and j-axis radial forces and is one of the inputs. The other input is $\boldsymbol{i}_m$. Some parameters as M_d' or M_q' have been considered also inputs in a vector. Applying the equation (56), implemented in a MATLAB function, the suspension current reference vector, $\boldsymbol{i}_{s,ref}$, is obtained as output.

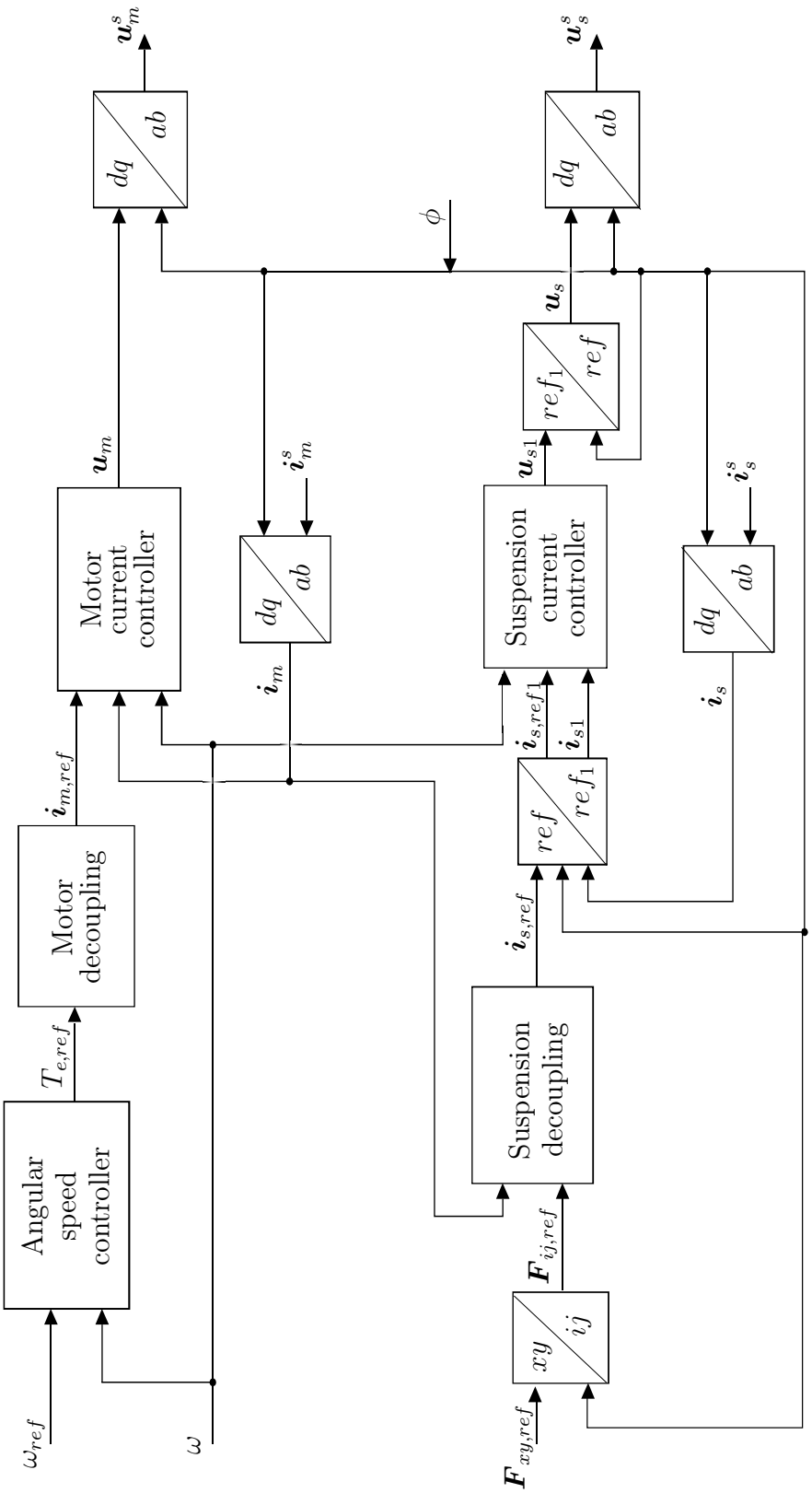

Figure 19: Vector control.

4.2.4 Motor current controller

The procedure described in Section 3.3 has been followed for the implementation of the motor current controller. Equations (37), (39), (49), (51) and (52) have been considered. Figure 20 shows the interior of the block developed. The variables $\boldsymbol{i}_{m,ref}$, $\boldsymbol{i}_m$ and ω are the inputs and the output obtained is $\boldsymbol{u}_m$. This voltage is transformed later from rotating to stationary coordinates and it will be one of the outputs of the *Vector control* block that becomes an input for the *BSyRM and mechanics* block.

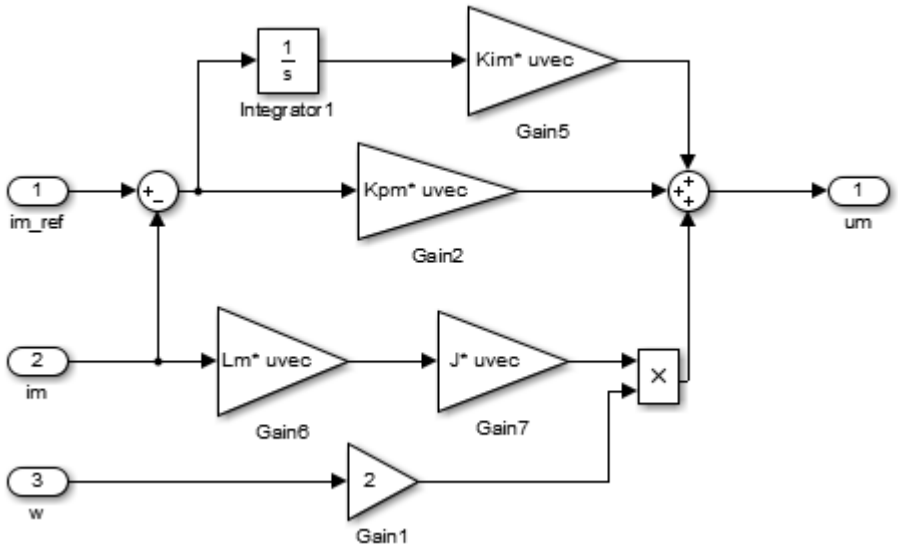

Figure 20: Motor current controller.

4.2.5 Suspension current controller

The suspension current controller implementation also follows the procedure described in Section 3.3. Equations (38), (40), (50), (53) and (54) have been considered. Figure 21 shows the suspension current controller developed. In this block, the inputs are $\boldsymbol{i}_{s,ref}$, $\boldsymbol{i}_s$ and ω, and the output obtained is $\boldsymbol{u}_s$. As it happened with the motor voltage space vector $\boldsymbol{u}_m$, the current voltage space vector $\boldsymbol{u}_s$, will be transformed from rotating to stationary coordinates and it will become one of the outputs of the *Vector control* block that becomes an input for *BSyRM and mechanics* block.

In Figure 21, it can be observed that the currents and the voltage have the subscript *1*. This is because before entering into the *Suspension current controller* block, the inputs $\boldsymbol{i}_{s,ref}$ and $\boldsymbol{i}_s$ have an intermediate transformation. In this new reference frame, the vectors are constant in steady state. The same happens with the output $\boldsymbol{u}_s$, that have to be transformed to undo the previous intermediate transformation and go back to the rotating reference frame. This transformation can be seen in Figure 19,

in the blocks ref/ref_1 and ref_1/ref located before and after the *Suspension current controller* block.

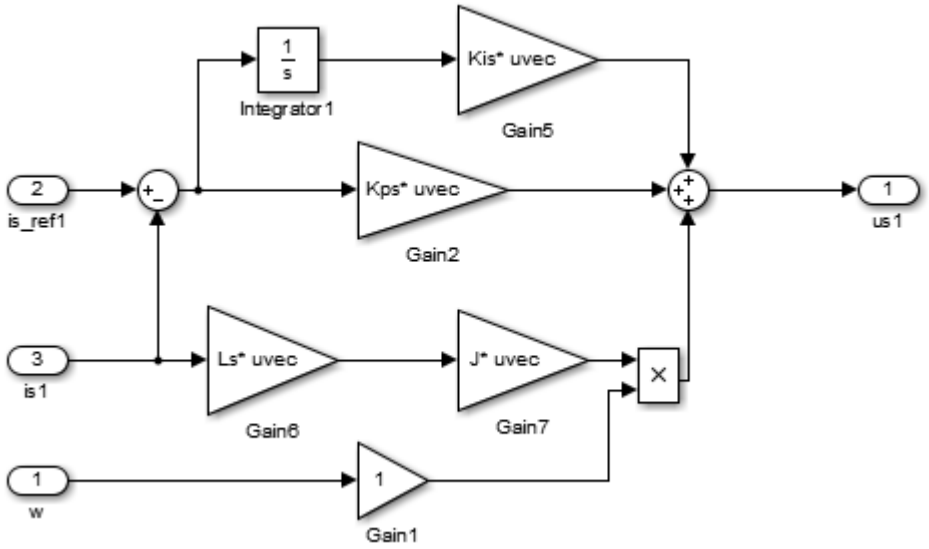

Figure 21: Suspension current controller.

5 Simulation results

Different cases have been tested with the Simulink model developed. In each case, various waveforms are shown to verify the correct operation of the machine and its control.

Figure 22 shows a chart of the main level of the Simulink model. As mentioned before, it can be seen that the model consists of two principal blocks, the *Vector control* and the *BSyRM and mechanics*. These two blocks are interconnected and they have different inputs. To simulate different operation points of the BSyRM, the red inputs shown in the figure (*Speed reference*, *Force reference* and x, y variables), will be modified. Constant values or steps are used as inputs for these variables. Concerning the load torque, all the simulations have been done with no load torque, i.e. the load torque is zero in every case.

Three different cases are studied. In each case, the description of the inputs that have been chosen and the analysis of the most interesting waveforms obtained when testing the Simulink model are provided.

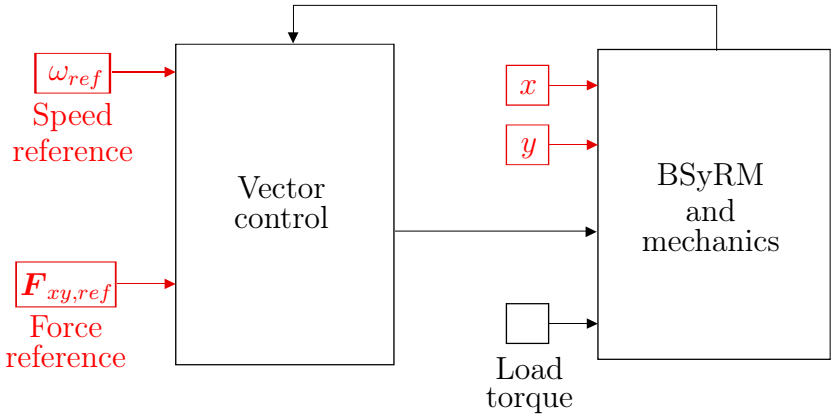

Figure 22: Simulink model.

5.1 Case 1

In the first simulation, a step has been chosen as a speed reference. This step has a step time of 0.1 seconds and a final value of $5000\frac{2\pi}{60}$ rad/s. Constant values have been chosen for the force references, $F_{x,ref} = 5$ N, $F_{y,ref} = 2$ N, and for the rotor displacement $x = y = 1$ μm.

Figure 23 includes the speed and force waveforms. In the speed graph, it can be seen the step that has been introduced in the reference speed ω_{ref} at 0.1 seconds. In this instant, the speed ω starts to grow until it reaches the final value of the step, following the reference. In the force graph it can be observed that the forces F_x and F_y follow the references, but at 0.1 seconds because of the speed step there is a deviation from the force reference values. This deviation is solved quickly and the forces continue following their corresponding references. This is a proof of the right

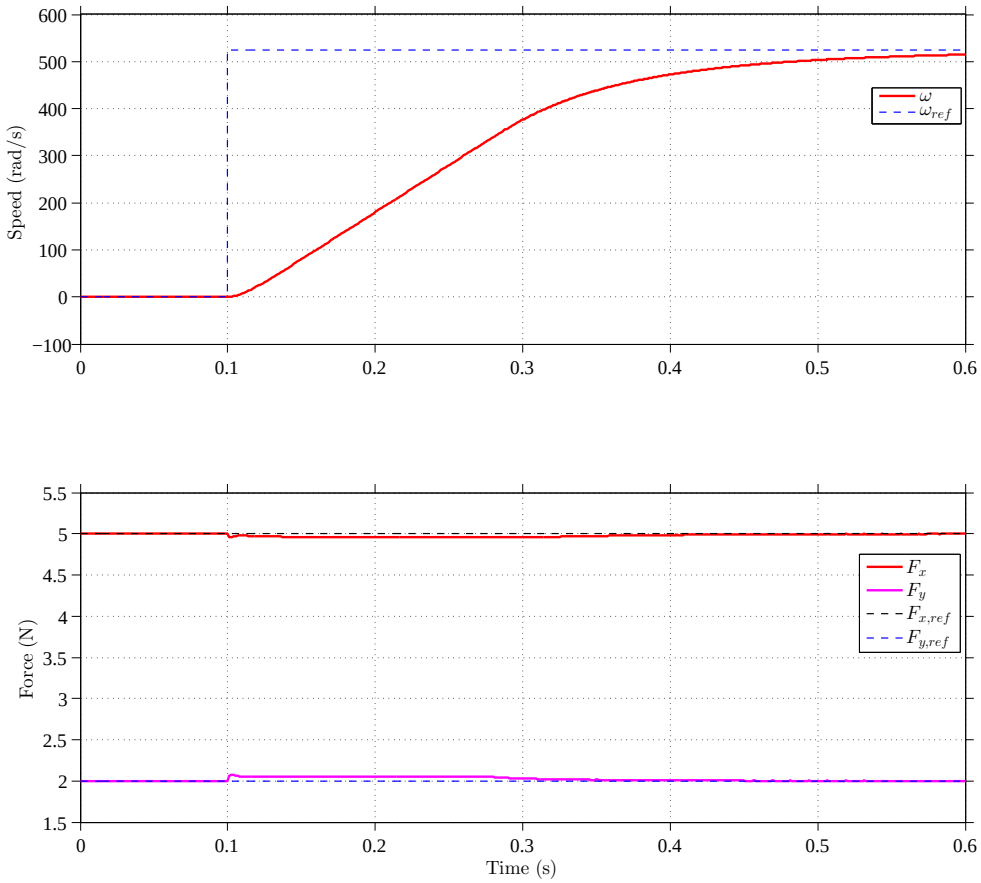

Figure 23: Simulation 1: The figure includes the speed and force waveforms.

operation of the control developed.

Figure 24 shows the waveforms of motor currents and suspension currents. The currents of the two first waveforms are in rotating coordinates, while the currents of the two last waveforms are in stationary coordinates. In the first graph it can be seen that the d-axis motor current i_{md} follows the reference $i_{md,ref} = 8$ A. The q-component of the motor current also follows the reference, adapting to the reference after the step. The other three graphs show how the waveforms reach the steady state after the step. The variables are followings the references in every case, what means the control is working right.

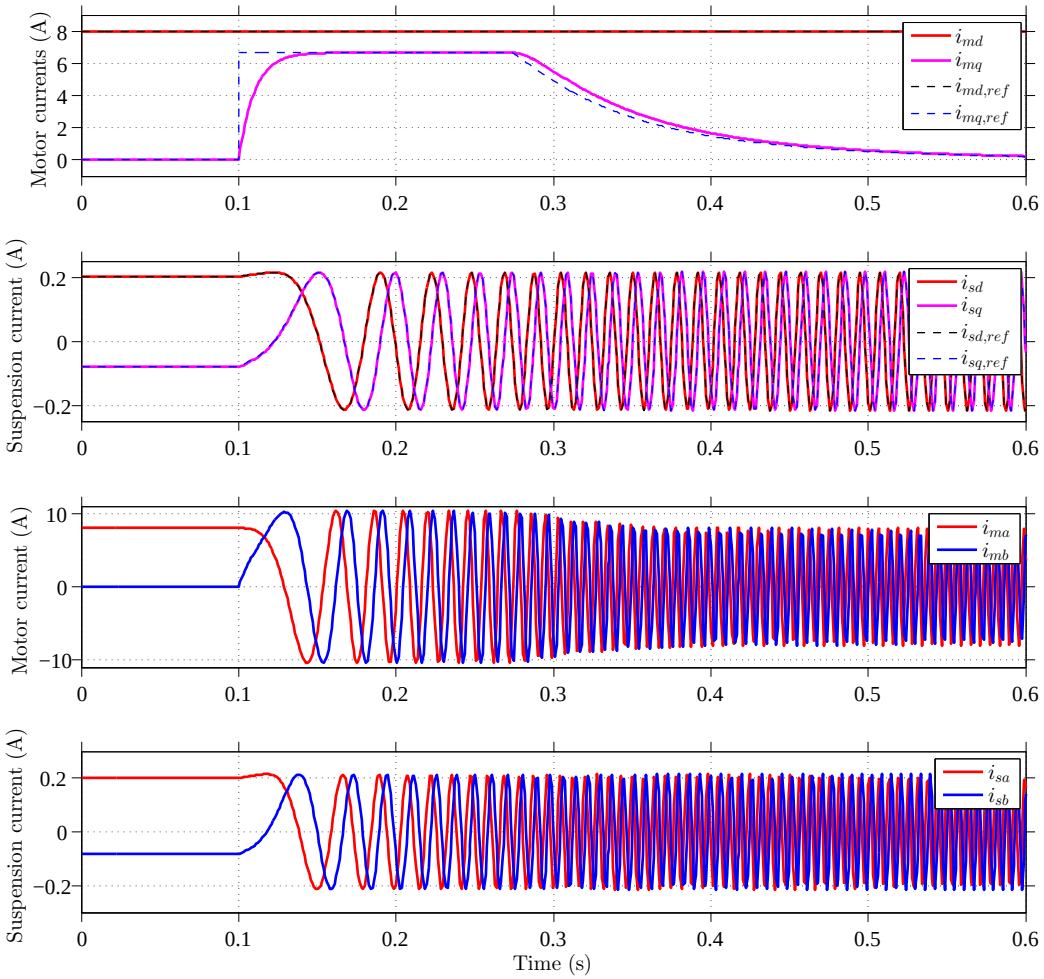

Figure 24: Simulation 1. The figure includes the motor and suspension currents waveforms.

5.2 Case 2

In the second simulation, the speed reference has a constant value of $5000\frac{2\pi}{60}$ rad/s. The inputs of the force references are also constants, $F_{x,ref} = 5$ N and $F_{y,ref} = 2$ N. In this case the step is used in the x-axis rotor displacement. The step has a step time of 0.05 seconds and a final value of 1 μm. The y-axis rotor displacement has a constant value of 1 μm.

Figure 25 shows the waveforms of the speed, force, motor currents and suspension currents. The speed and the motor current do not suffer any disturbance when the step is introduced in the x-axis rotor displacement, what shows that there is no relationship between the rotor displacement and the speed and motor current. The force and the suspension current experience a deviation at 0.05 seconds. When a step is introduced in the x-axis rotor displacement, the forces must act to solve this disturbance, that is the reason why the forces suffer a change at 0.05 seconds. The relationship between the deviation in the force and in the suspension current can be explained using equations (20) and (21). This deviation is solved immediately and the signals continue following the references.

These results are related to the fact why the flux distributions excited by suspension windings depend on the rotor radial displacements, even though these displacements are small. However, although in real machines some coupling probably appears, the flux distributions of motor windings are not affected by the rotor radial displacement in the studied case. [5]

5.3 Case 3

In the third simulation, the speed reference has a constant value of $5000\frac{2\pi}{60}$ rad/s. The step is used as the input of the force reference. In both cases, $F_{x,ref}$ and $F_{y,ref}$, the step time is 0.05 seconds. The final value of the x-axis force reference is 3 N and the final value of the y-axis force reference is 10 N. The rotor displacement chosen is $x = y = 1$ μm.

Figure 26 includes the waveforms of the speed, force and motor and suspension currents. As in Case 2, the speed and the motor current do not suffer any deviation when the step is introduced, while the force and the suspension current experience a deviation from the reference. Again this prove the relationship between the force and the suspension current. After the disturbance the waveforms continue following the references verifying the right operation of the control implemented.

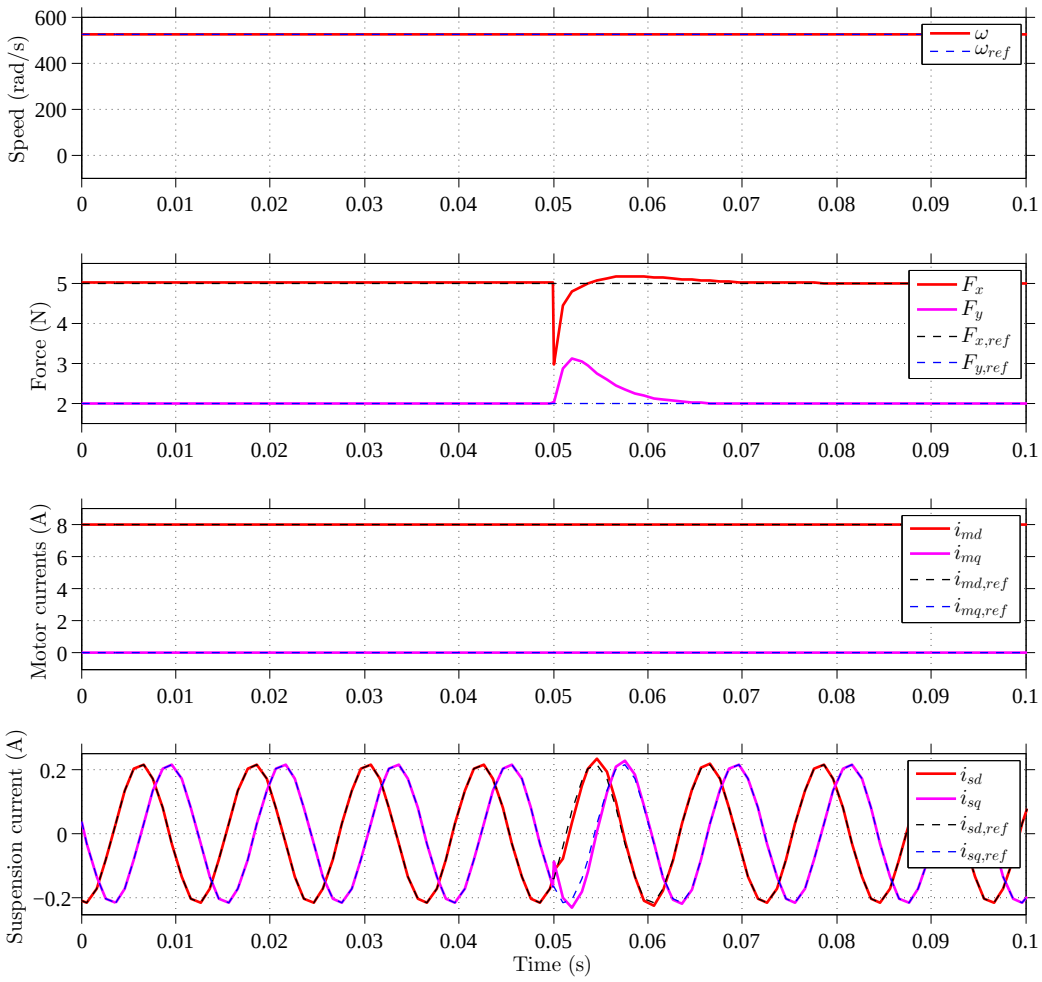

Figure 25: Simulation 2. The figure includes the speed, force, motor and suspension currents waveforms.

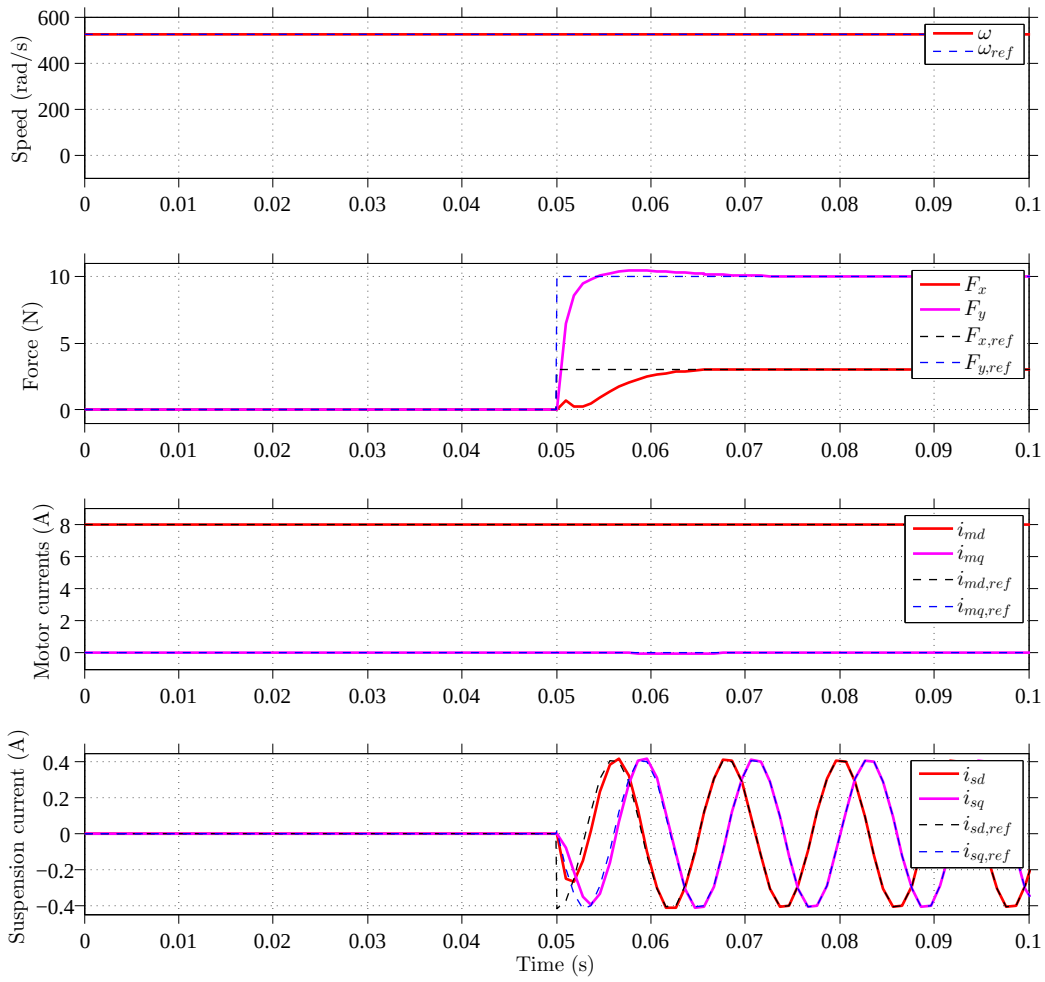

Figure 26: Simulation 3. The figure includes the speed, force, motor and suspension currents waveforms.

6 Conclusions

In this final project, a vector-controlled bearingless synchronous reluctance motor drive has been studied. Both the BSyRM dynamic model and vector control are explained in detail.

Due to the novelty of BSyRMs some difficulties have emerged during the realisation of this final project. The existence of additional suspension windings for generating the radial force has been one of the difficulties, making more difficult to obtain the dynamic model equations. Due to the shortage of these motor types, other problem has been to find the appropriate machine parameters that permit to simulate the operation of the motor.

To obtained the dynamic model equations of the BSyRM, more general PMSM equations have been used as a starting point. Later these equations have been refined to suit the particular feature of the BSyRM.

In this study of BSyRMs, the magnetic saturation has not been taken into consideration to simplify the model. In bearingless motors, one important drawback is the coupling between motor and bearing system by magnetic saturation. The saturation can lead to an unstable system performance. Therefore, further studies will include the modelling of the magnetic saturation.

Improvements to the suspension current controller could be made, but it was considered outside the scope of this final project. However, the suspension current controller should be developed more precisely in later studies. PI-controller parameters values could also have been further tuned.

To verify the correct operation of the BSyRM model developed, several simulations have been tested using the Matlab/Simulink software. The simulation results presented, verify that the dynamic model of the BSyRM and the vector control implemented, perform well.

References

[1] T. Fukao. The evolution of motor drive technologies, development of bearingless motors. In *The Third International Power Electronics and Motion Control Conference. (IPEMC 2000). Proceedings*, volume 1, pages 33–38 vol.1, 2000.

[2] Zengcai Qu, T. Tuovinen, and M. Hinkkanen. Inclusion of magnetic saturation in dynamic models of synchronous reluctance motors. In *2012 XXth International Conference on Electrical Machines (ICEM 2012)*, pages 994–1000, Sept 2012.

[3] A. Boglietti, A. Cavagnino, M. Pastorelli, and A. Vagati. Experimental comparison of induction and synchronous reluctance motors performance. In *Fourtieth IAS Annual Meeting. Conference Record of the Industry Applications Conference*, volume 1, pages 474–479 Vol. 1, Oct 2005.

[4] A. Chiba, M. Hanazawa, T. Fukao, and M. Azizur Rahman. Effects of magnetic saturation on radial force of bearingless synchronous reluctance motors. *IEEE Transactions on Industry Applications*, 32(2):354–362, Mar 1996.

[5] A. Chiba, T. Deido, T. Fukao, and M.A. Rahman. An analysis of bearingless ac motors. *IEEE Transactions on Energy Conversion*, 9(1):61–68, Mar 1994.

[6] C. Michioka, T. Sakamoto, O. Ichikawa, A. Chiba, and T. Fukao. A decoupling control method of reluctance-type bearingless motors considering magnetic saturation. *IEEE Transactions on Industry Applications*, 32(5):1204–1210, Sept 1996.

[7] A. Chiba, M.A. Rahman, and T. Fukao. Radial force in a bearingless reluctance motor. *IEEE Transactions on Magnetics*, 27(2):786–790, Mar 1991.

[8] Hannian Zhang, Huangqiu Zhu, Zhibao Zhang, and Zhiyi Xie. Design and simulation of control system for bearingless synchronous reluctance motor. In *Proceedings of the Eighth International Conference on Electrical Machines and Systems. (ICEMS 2005)*, volume 1, pages 554–558 Vol. 1, Sept 2005.

[9] Xiaodong Sun, Long Chen, and Zebin Yang. Overview of bearingless permanent-magnet synchronous motors. *IEEE Transactions on Industrial Electronics*, 60(12):5528–5538, Dec 2013.

[10] A. Chiba, T. Fukao, O. Ichikawa, M. Oshima, M. Takemoto, and D.G. Dorrell. *Magnetic Bearings and Bearingless Drives*. Elsevier, Newnes, GBR, 2005. ISBN 0 7506 5727 8.

[11] M. Takemoto, K. Yoshida, N. Itasaka, Y. Tanaka, A Chiba, and T. Fukao. Synchronous reluctance type bearingless motors with multi-flux barriers. In *Power Conversion Conference - Nagoya. (PCC 2007)*, pages 1559–1564, April 2007.

[12] M. Hinkkanen. Control of electric drives. Course material, Aalto University. Helsinki, Finland, 2013.

[13] H. Van Khang, Jang-Mok Kim, Jin-Woo Ahn, and Hui Li. Synchronous reluctance motor drive system parameter identification using a current regulator. In *Twenty-Third Annual IEEE Applied Power Electronics Conference and Exposition. (APEC 2008)*, pages 370–376, Feb 2008.

[14] Yuanfei Li, Xiaodong Sun, and Huangqiu Zhu. Parameter design and fem analysis on a bearingless synchronous reluctance motor. *Lecture Notes in Electrical Engineering*, 98:163–171, 2011.

[15] L. Hertel and W. Hofmann. Magnetic couplings in a bearingless reluctance machine. Compendium, Department of Electrical Machines and Drives. Technical University of Chemnitz. Chemnitz, Germany.

[16] L. Harnefors. Control of variable-speed drives. Compendium, Mälardalen University. Västerås, Sweden, 2003.

[17] Lennart Harnefors and H-P Nee. Model-based current control of ac machines using the internal model control method. *IEEE Transactions on Industry Applications*, 34(1):133–141, Jan 1998.

A Appendix

A.1 Simulink dynamic model

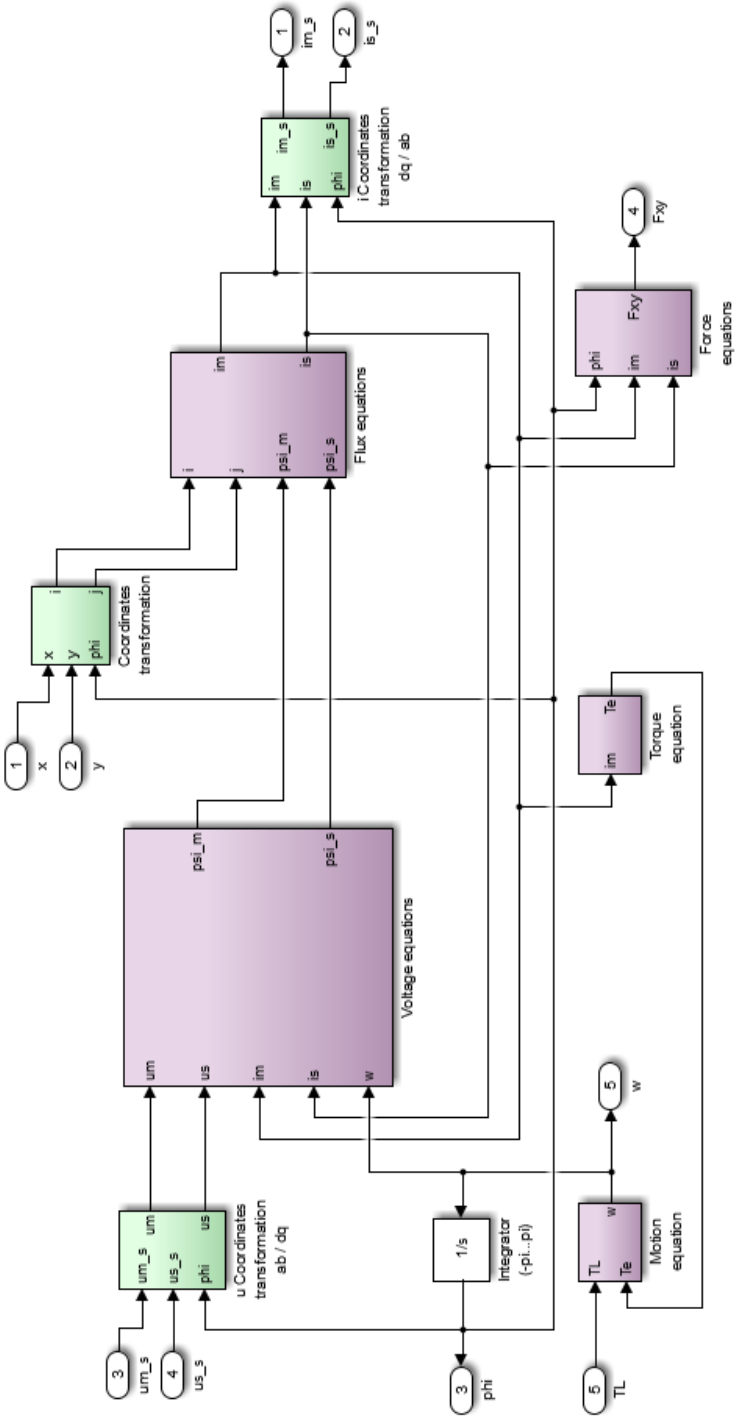

Figure A1: Dynamic model of the machine.

A.1.1 Flux equations

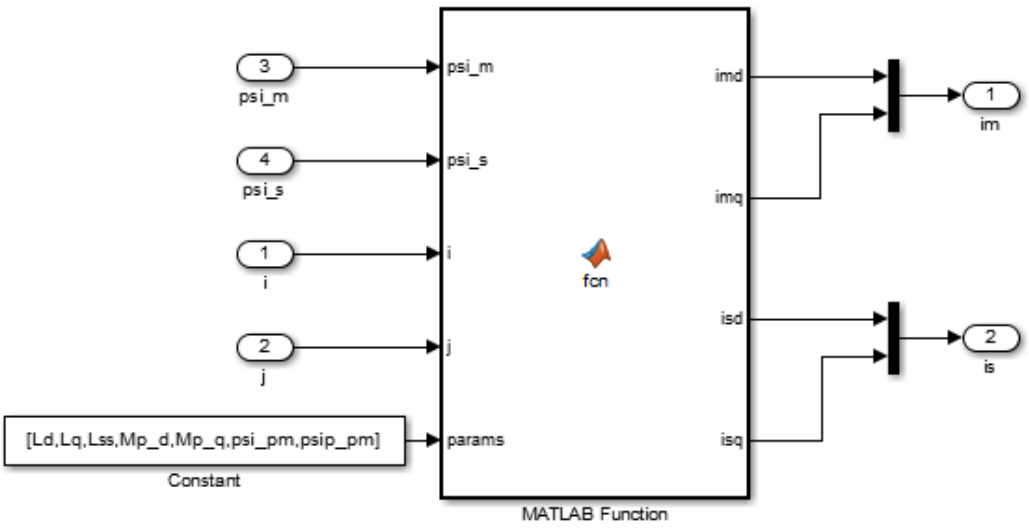

Figure A2: Flux equations block.

The code implemented in the flux MATLAB function is:

```
function [imd,imq,isd,isq] = fcn(psi_m,psi_s,i,j,params)

%Paramenters
Ld = params(1);
Lq = params(2);
Lss = params(3);
Md = params(4);
Mq = params(5);
psi_pm = params(6);
psi_pmp = params(7);

%Matrices and vectors definitions
Lm = [Ld, 0; 0, Lq];
Ls = [Lss, 0; 0, Lss];
M = [Md*i, -Md*j; Mq*j, Mq*i];
psi_pmpv = [psi_pmp*i; -psi_pmp*j];
psi_pmv = [psi_pm; 0];

%Currents as a function of flux linkages
is = (Ls - M.'/Lm*M)\(psi_s - psi_pmpv - M.'/Lm*(psi_m - psi_pmv));
im = Lm\(psi_m - psi_pmv - M*is);
isd = is(1);
isq = is(2);
imd = im(1);
imq = im(2);
```

A.1.2 Torque equation

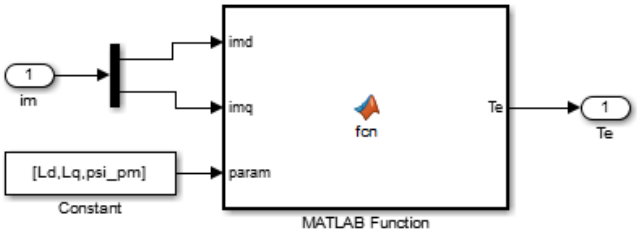

Figure A3: Torque equation block.

The code implemented in the torque MATLAB function is:

```
function Te = fcn(imd,imq,param)

%Parameters
Ld = param(1);
Lq = param(2);
psi_pm = param(3);

%Torque equation
Te = 3*((Ld-Lq)*imd*imq + psi_pm*imq);
```

A.1.3 Motion equation

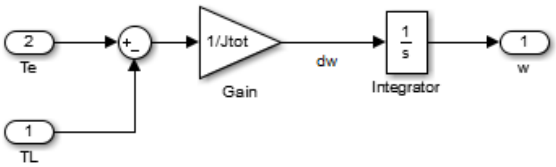

Figure A4: Motion equation block.

A.2 Simulink vector control model

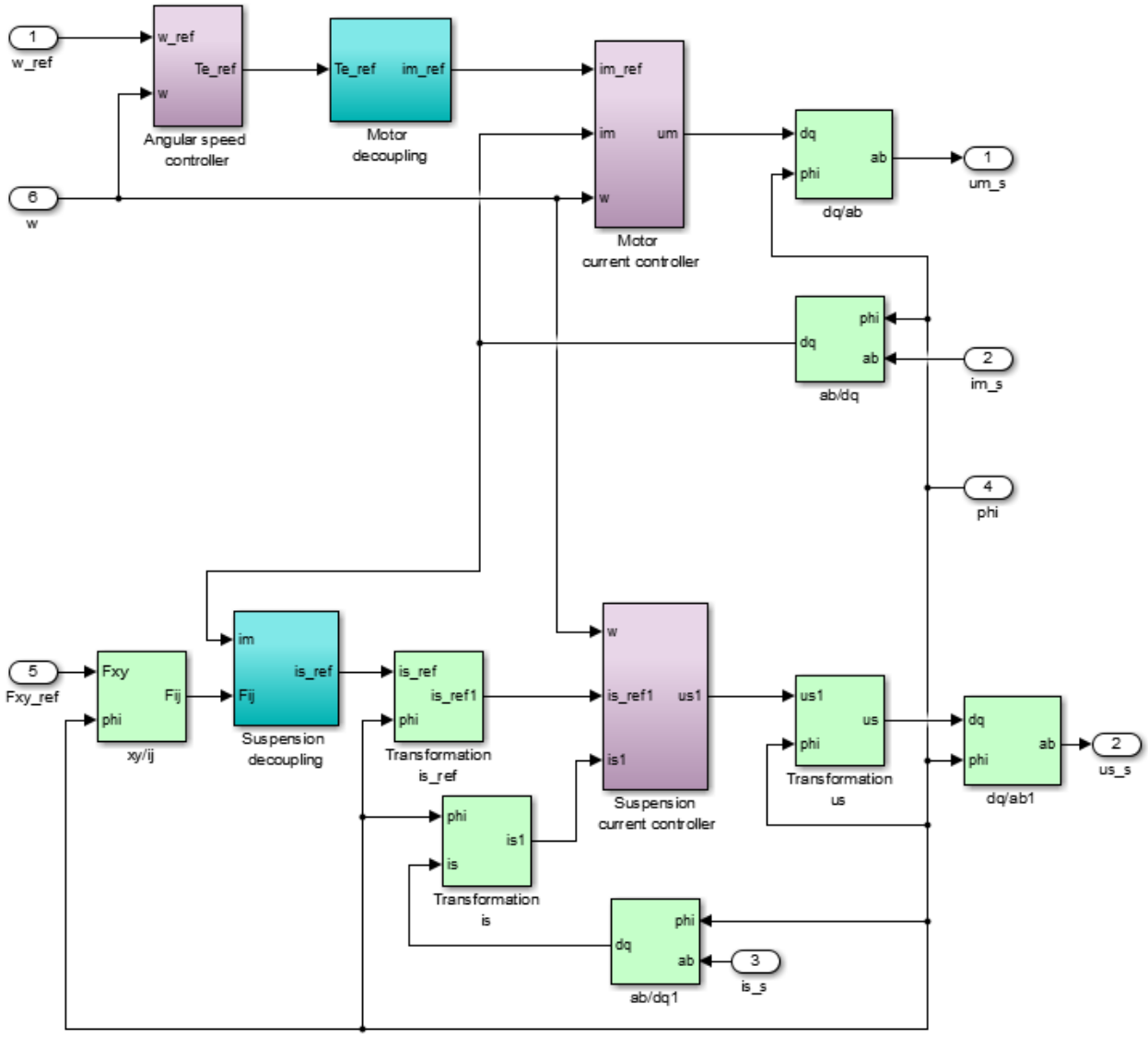

Figure A5: Vector control of the machine.

A.2.1 Angular speed controller

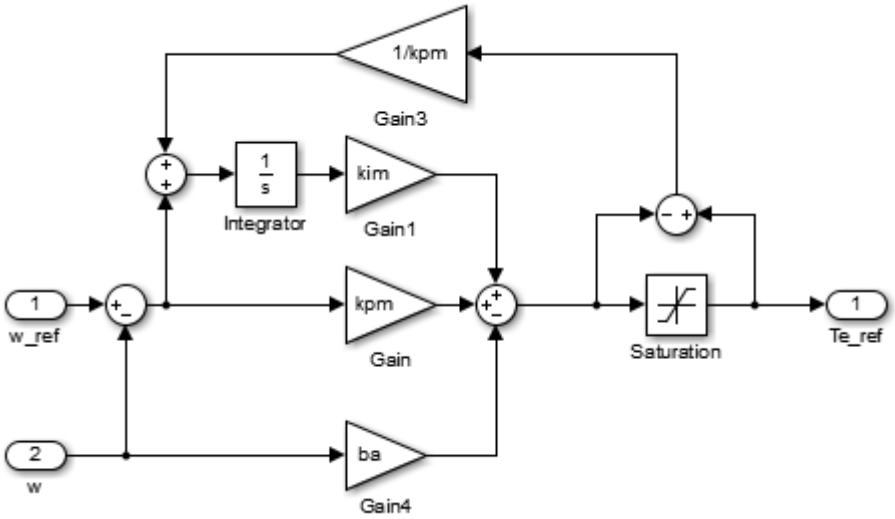

Figure A6: Angular speed controller.

A.2.2 Motor decoupling

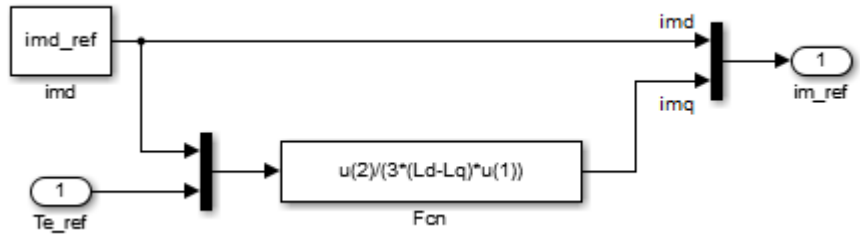

Figure A7: Motor decoupling.

A.2.3 Suspension decoupling

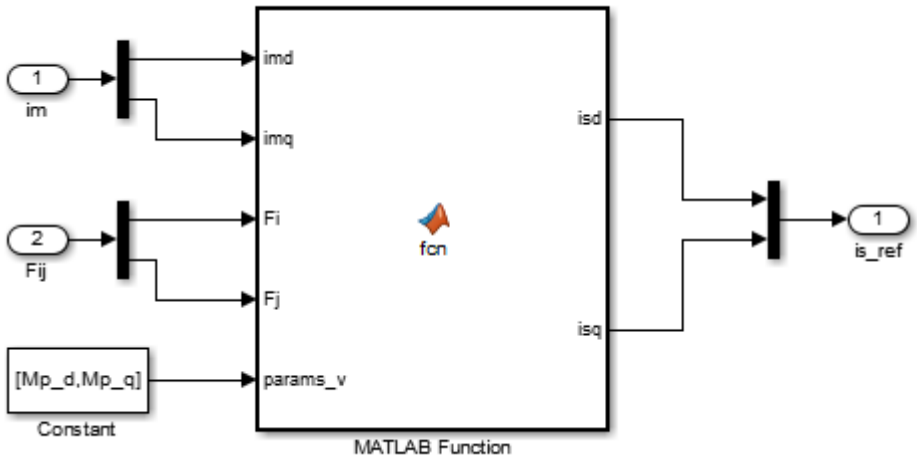

Figure A8: Suspension decoupling.

The code implemented in the suspension decoupling MATLAB function is:

```
function [isd,isq] = fcn(imd,imq,Fi,Fj,params_v)

%Paramenters
Mp_d = params_v(1);
Mp_q = params_v(2);

%Equation
D = ((Mp_d*imd)^2)+((Mp_q*imq)^2);

if  (D > 100*eps)

   isd = (Mp_d*imd*Fi+Mp_q*imq*Fj)/D;
   isq = (Mp_q*imq*Fi-Mp_d*imd*Fj)/D;

else

   isd = 0;
   isq = 0;

end
```